Palaeogeography, Palaeoclimatology, Palaeoecology 627 (2023) 111741

Contents lists available at ScienceDirect

Palaeogeography, Palaeoclimatology, Palaeoecology

journal homepage: www.elsevier.com/locate/palaeo

A lithostratigraphic reappraisal of a Permian-Triassic fluvial succession at Allan Hills (Antarctica) and implications for the terrestrial end-Permian extinction event

Gianluca Cornamusini [a,b,c], Luca Zurli [a,*], Giovanni P. Liberato [a], Valentina Corti [a], Erik L. Gulbranson [d], Matteo Perotti [a], Sonia Sandroni [c,e]

[a] Department of Physical, Earth, and Environmental Sciences, University of Siena, via Laterina 8, 53100 Siena, Italy
[b] Centre for GeoTechnologies, University of Siena, Via Vetri Vecchi 34, San Giovanni Valdarno (AR), 52027, Italy
[c] Museo Nazionale dell'Antartide, University of Siena, Via Laterina 8, 53100 Siena, Italy
[d] Department of Environment, Geography, and Earth Sciences, Gustavus Adolphus College, 800 W. College Ave, St. Peter, MN 56082, USA
[e] Istituto Nazionale di Geofisica e Vulcanologia – Pisa section, Via C. Battisti 53, 56125 Pisa, Italy

ARTICLE INFO

Keywords:
Gondwana
Southern Victoria Land
Stratigraphy
Permian-Triassic boundary
Beacon Supergroup
Allan Hills

ABSTRACT

Between Permian to Triassic, the Earth experienced climatic and biotic crises, included the greatest mass extinction at the Permian-Triassic boundary. These climatic and biological changes are reflected in both marine and terrestrial depositional systems. Over this time span, the Gondwana supercontinent hosted numerous large basins that may preserve the paleoenvironment response to global changes in the sedimentary record. This study provides a lithostratigraphic reappraisal of the latest Paleozoic-Mesozoic alluvial Beacon Supergroup at Allan Hills (Convoy Range), which is one of the most complete sedimentary sequences in Antarctica. Fieldwork stratigraphic-lithological observation, facies analysis, and petrographic characterization of sedimentary rocks allow the identification of six depositional units. The investigations point out for a conformable relationship between depositional and lithostratigraphic units, characterized by changes in the fluvial style. The reconnaissance of a "transitional interval" showing intermediate features between the Permian Weller Coal Measures and the Triassic Feather Conglomerate strengthen the conformable nature of the sequence across the Permian-Triassic boundary in this region. The lithological features of such interval strongly resemble those observed in the coeval deeply studied Eastern Australia successions crossing the Permian-Triassic boundary as well as the end-Permian extinction event. More precisely, the uppermost coal occurrence, just above a glossopterid macroflora-bearing carbonaceous mudstone within the "transitional interval", marks the disappearance of coal-peat forming Permian vegetation which corresponds with the terrestrial end-Permian extinction, thus representing one of the few end-Permian extinction records in Antarctica.

1. Introduction

During the Late Paleozoic, the Earth experienced severe changes in climatic and biotic evolution from a series of greenhouse gas-forced and eccentricity-paced glaciations/deglaciations during the Late Paleozoic Ice Age, which involved most of Gondwana (see Montañez, 2022 for a synthesis). The Late Paleozoic culminates with the most severe mass extinction in the history of metazoan life. This mass extinction, the end-Permian extinction (EPE), is linked with significant climate forcings, subaerial volcanism and included significant alterations to ecosystems in the marine and terrestrial realms. However, high-precision geochronology indicates that the terrestrial EPE occurred just prior to the Permian-Triassic boundary (PTB; see Fielding et al., 2019), indicating that environmental and climatic upheavals were sustained on ca. 300 kyr timescales. The transition to the PTB is characterized by global-scale geological events, i.e., the Siberian Traps Large Igneous Province, that led to dramatic greenhouse gas emissions, which deeply modified the global climate with an intense warming (Brand et al., 2012; Payne and Clapham, 2012; Song et al., 2014; Burgess et al., 2017; Dal Corso et al., 2020; Wu et al., 2021). The response of biosphere to these climatic changes resulted in the greatest mass extinction of the Earth history, the EPE, that in the marine realm is dated at 251.9 Ma (Burgess et al., 2014),

* Corresponding author.
E-mail address: luca.zurli@unisi.it (L. Zurli).

https://doi.org/10.1016/j.palaeo.2023.111741
Received 17 February 2023; Received in revised form 19 July 2023; Accepted 21 July 2023
Available online 25 July 2023

while within the continental environment, the timing of the mass extinction and the response of the sedimentary systems are more articulated and still debated. Indeed, new advances have been carried out on the PTB/EPE in Australia, South Africa, and China revealing a floristic turnover in response to drastic environmental changes, which predates the marine mass extinction (Fielding et al., 2019; Gastaldo et al., 2020; Mays et al., 2020; Lu et al., 2022).

In this study, we approach one of the best exposed Permian-Triassic succession of the Victoria Land Basin in Antarctica, to evaluate the stratigraphic-depositional changes and to recognize the EPE through the sedimentary record. New data provided here integrate data across the Antarctic Beacon Supergroup successions, facilitating comparisons with other Gondwana continental basins.

The approach here used has been the selection of well-exposed Permian-Triassic successions at Allan Hills in the Convoy Range area of southern Victoria Land (SVL) along the Transantarctic Mountains (TAM; Fig. 1). Detailed lithostratigraphic field surveys, to obtain a well-constrained map for an updated stratigraphic-depositional framework, were performed. Detailed sedimentological and petrographic investigations provide crucial observations that inform the interpretations of this stratigraphic-depositional framework.

In this regard, it is necessary to: i) reappraise the lithostratigraphic setting of the Victoria Group; ii) elucidate broad regional stratigraphic surfaces through a new geological map of the deglaciated area of Allan Hills; iii) systematically record the main lithological and sedimentological features; and iv) describe the bounding depositional unit surfaces, with a focus on the terrestrial end-Permian extinction event and the Permian-Triassic boundary.

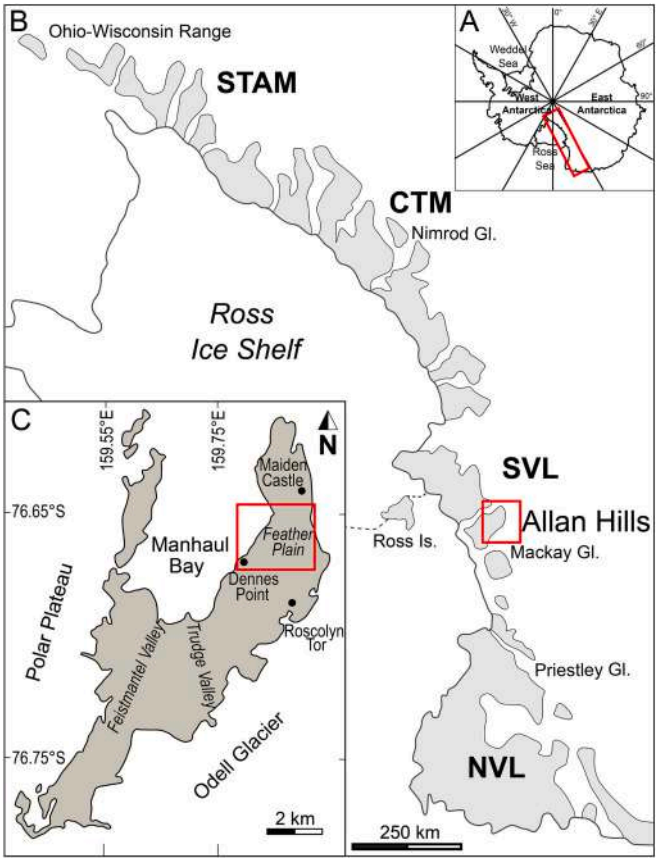

Fig. 1. A) Map of Antarctica. Red box enlarged in B; B) Ross Sea Embayment with grey areas representing the partially deglaciated regions. Red box enlarged in C. Gl.: Glacier; Is.: Island; C) map of the Allan Hills nunatak. Red box shows the study area. STAM: southern Transantarctic Mountains; CTM; Central Transantarctic Mountains; SVL: southern Victoria Land; NVL: northern Victoria Land. (For interpretation of the references to colour in this figure legend, the reader is referred to the web version of this article.)

2. Regional and geological setting

Along the TAM, a ca. 3500 km long mountain range, an extensive and thick Late Paleozoic–mid Mesozoic sedimentary cover unconformably lies on crystalline basement. It represents the resumption of sedimentation in southern Gondwana following a long time-gap between Precambrian–early Paleozoic orogenesis and subsequent dismantling of this orogenic belt (see Goodge, 2020 for a review). Coeval and similar deposits widely occur across the continents constituting the southern portion of Gondwana, such as: Australia, South America, and southern Africa (Barrett, 1981, 1991; Collinson et al., 1994; Elliot, 2013). This succession, named Beacon Supergroup in Antarctica, ranges widely in thickness from ca. 100 to 2500–3000 m.

The Beacon Supergroup strata unconformably overlie an important erosional surface (Kukri Erosion Surface) onto the crystalline basement referred to the latest Proterozoic-early Paleozoic Ross Orogen (Barrett, 1991; Stump, 1995; Cox et al., 2012; Elliot, 2013). The basement is mainly made up of igneous rocks of the Granite Harbour Intrusive Complex, and high- to very low-grade metamorphic rocks (Stump, 1995; Cox et al., 2012; Goodge, 2020). The Beacon Supergroup mainly consists of terrestrial siliciclastic sediments, mostly sandstone, mudstone, and minor conglomerate, deposited in an alluvial environment, with minor depositional intervals recording glacial and shallow-marine paleoenvironments (Barrett and Kohn, 1975; Barrett, 1991; Isbell and Cúneo, 1996; Gulbranson et al., 2020).

In SVL the Beacon Supergroup shows a subdivision into two groups (Fig. 2): the Devonian Taylor Group and the uppermost Carboniferous-Lower Jurassic Victoria Group. The Taylor and Victoria groups are separated by an erosional surface (Maya Erosion Surface).

The Taylor Group in SVL is up 1400 m thick, subdivided into eight lithostratigraphic formations (Cox et al., 2012) while the Victoria Group, disconformably overlying it, is subdivided into six formations (Cox et al., 2012). In the whole, the Victoria Group reaches a maximum thickness of ca. 1000 m, overlain by Lower Jurassic basalts and volcaniclastic deposits of the Ferrar Group (Barrett, 1991; Stump, 1995; Elliot, 2013).

The study area of this research is the Allan Hills nunatak; the stratigraphy was previously discussed by Gunn and Warren (1962), Borns and Hall (1969), and Ballance (1977); Fig. 3 shows the geological map of the investigated area. Four lithostratigraphic formations of the Victoria Group crop out: Weller Coal Measures, Feather Conglomerate, Lashly Formation, and Mawson Formation (Harrington, 1965; Barrett, 1991; Smith et al., 1998; Elliot et al., 2006; Gulbranson et al., 2020).

The Weller Coal Measures Formation (Webb, 1963; McElroy, 1969) is divided into three members; this study investigated the uppermost one consisting of sandstone-dominated deposits with interlayers of coal, carbonaceous mudstone, and siltstone of Early-Middle Permian age following older authors (middle Artinskian to early Roadian; Kyle, 1977; Kyle and Schopf, 1982; Farabee et al., 1990; Askin, 1997). However, recent studies indicate a Middle-Late Permian palynological assemblage in the Allan Hills sequences (Awatar et al., 2014; Corti, 2021). Regionally, the Weller Coal Measures are a correlative unit to the Buckley Formation in central Transantarctic Mountains, and the Takrouna Formation in northern Victoria Land (Fig. 2), both extending to the Late Permian (Elliot, 2013; Bomfleur et al., 2021).

The Weller Coal Measures pass upwards to the Feather Conglomerate, a ca. 80 m thick succession, that contains thick coarse sandstone beds, subdivided as the Mt. Fleming Member in the upper portion by an increase of mudstone interlayers (Barrett et al., 1971). The Feather Conglomerate is barren of megafossil remnants useful for an age-dating; Kyle (1977) and Kyle and Schopf (1982) proposed a Late Permian age, while Retallack et al. (2005), based on paleopedological data, suggested an Early Triassic age, with which recent data from Gulbranson et al.

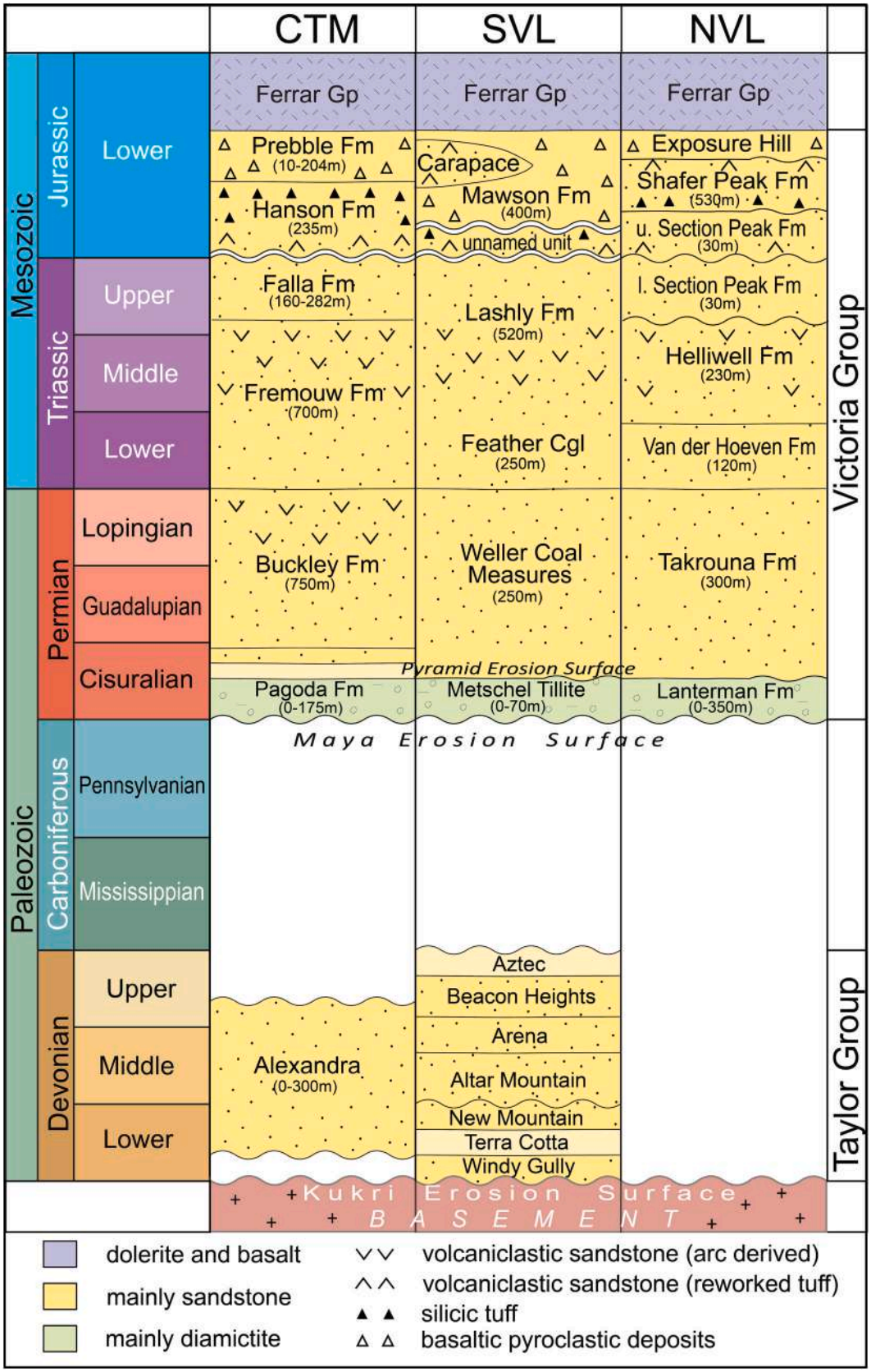

Fig. 2. Simplified stratigraphy of the Beacon Supergroup along the Transantarctic Mountains (modified from Zurli et al., 2022). Central Transantarctic Mountains stratigraphy is modified from Elliot, 2013; Elliot et al., 2017; Ives and Isbell, 2021. Southern Victoria Land stratigraphy is modified from Elliot, 2013, Liberato et al., 2017, and Ives and Isbell, 2021. Northern Victoria Land stratigraphy is modified from Cornamusini et al., 2017 and Bomfleur et al., 2021. Wavy lines are erosion surfaces. CTM: Central Transantarctic Mountains; SVL: southern Victoria Land; NVL: northern Victoria Land; Cgl: Conglomerate; Fm: Formation; Gp: Group; l.; lower; u.: upper.

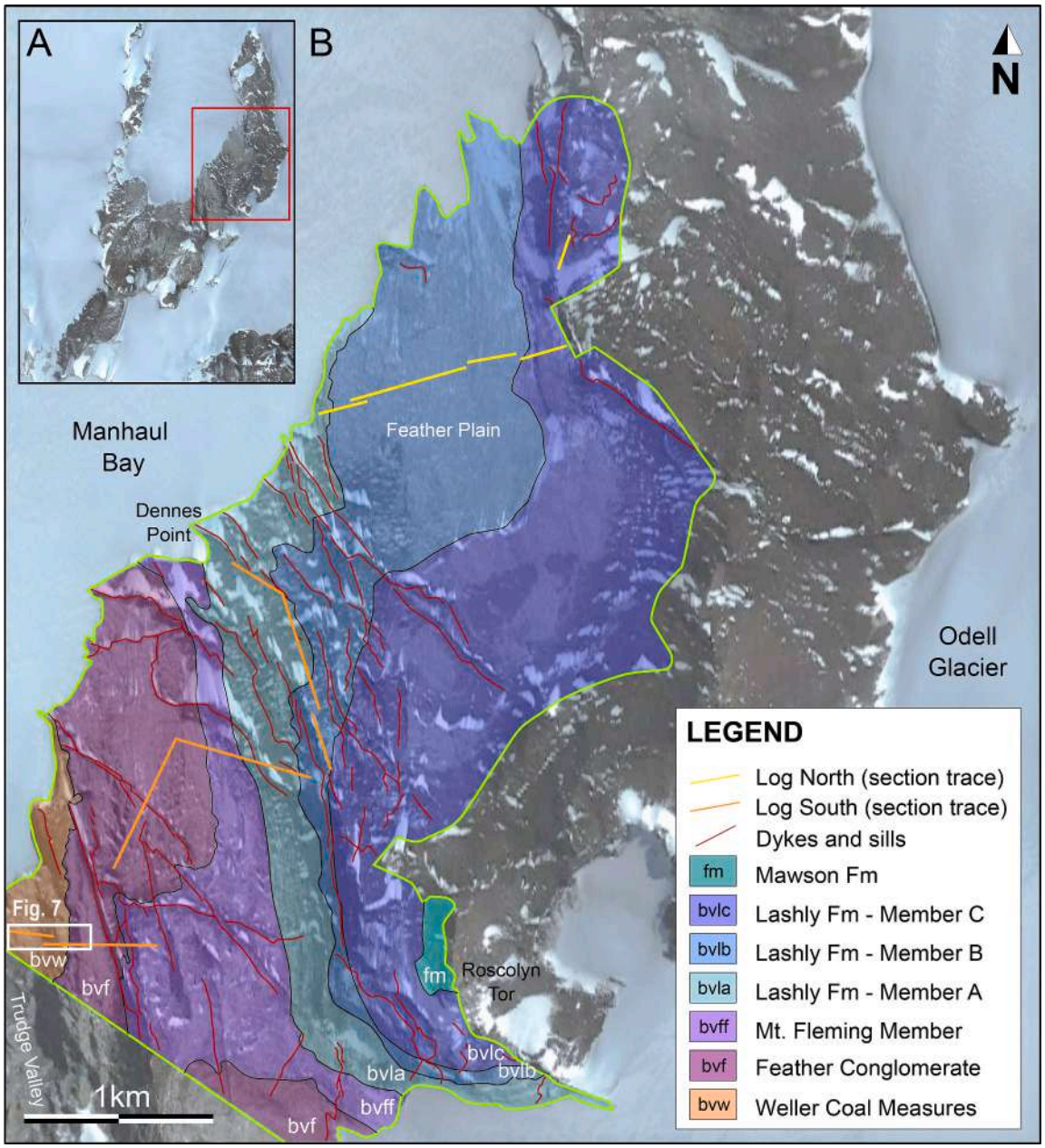

Fig. 3. A) Satellite image of the Allan Hills nunatak. Red box shows the study area; B) geological map of the studied sector of Allan Hills modified from Liberato et al. (2017). White box shows the traces of the detailed logs of Fig. 7. (For interpretation of the references to colour in this figure legend, the reader is referred to the web version of this article.)

(2020) are in accordance. The Feather Conglomerate was tentatively correlated with the Van der Hoeven Formation in northern Victoria Land which contains Early Triassic palynomorphs (Fig. 2; Bomfleur et al., 2021). The Mt. Fleming Member contains palynomorph assemblages referable to Early Triassic (Kyle, 1977; Barrett, 1981; Kyle and Schopf, 1982; Barrett and Fitzgerald, 1985).

The Lashly Fm., characterized by alternating sandstone and mudstone rich in fossil wood and/or coal, overlies the Feather Conglomerate and is subdivided into four members (A to D from the oldest) on the base of the sandstone/mudstone ratio (Barrett and Webb, 1973; Barrett and Kohn, 1975). Kyle (1977) and Kyle and Schopf (1982), based on palynomorph assemblages, attributed Member A (as well as the upper part of the Mt. Fleming Mb.) to the subzone A and to the lower part of the subzone B of the *Alisporites* Zone (late Early Triassic to lowest Middle Triassic), confirmed by recent U—Pb calibrated palynozones in the Sydney Basin (Fielding et al., 2019; Mays et al., 2020); the Member B to subzone B and the lowermost part of the subzone C of the *Alisporites* Zone (Middle Triassic to earliest Late Triassic), the Member C and the Member D respectively to the subzone C and subzone D of the *Alisporites* Zone (Late Triassic).

The Lashly Fm. is unconformably overlain by the Jurassic volcaniclastic Mawson Fm., with the Kirkpatrick Basalt on the top (Ballance and Watters, 1971). All the formations are intruded by dolerite dykes and sills of the Jurassic Ferrar Group, mainly N-S and NW-SE oriented (Fig. 3). The Mawson Fm. is well-exposed on the top of Roscolyn Tor and along its NE prolonging ridge (Fig. 3).

3. Materials and methods

This study focuses on some well-exposed sections cropping out at the Allan Hills in SVL (Fig. 1).

The approach here is field-based with large-scale observations

provided by detailed field mapping of the northeastern part of the Allan Hills nunatak (Fig. 3), with the reconstruction of the geometry of the mapped units. The field work was carried out during the 2012 to 2016 Italian PNRA (Programma Nazionale di Ricerche in Antartide) expeditions and 2012 to 2014 United States Antarctic Program (USAP) expeditions. These field expeditions provided the measurement of several stratigraphic logs representing ca. 800 m of thickness, with the collection of sandstone and mudstone samples. The high-resolution stratigraphic logs, traces of which are shown in Fig. 3, are here synthesized into two composite logs (Fig. 4): 1) the Log South (base at 76°41′43.84"S; 159°43′41.44″E), measured in the southern part of the study area; and 2) the Log North (base at 76°40′15.14"S; 159°48′52.60″E), which was measured in the northern part.

A classical lithostratigraphic approach was used during the fieldwork to define depositional-stratigraphic units. Sedimentological observations were made in the field, distinguishing the clastic deposits on the base of the sedimentary structures, geometry of the strata, paleocurrent data, and recognizing grain-size classes from clay to cobble.

The sedimentological and lithostratigraphic investigations allow identification of six depositional-stratigraphic units (Unit A to Unit F) to be compared with lithostratigraphic units. Facies analysis has been performed using the sedimentary facies scheme of Miall (2006) (Table S1) to define the facies architecture of the successions; facies were grouped into six facies associations (FA) on the basis of their features (Table 1). Each unit has been described on the basis of FA occurrence which allows the paleoenvironmental interpretations.

Compositional-petrographic analyses were carried out on 103 sandstone samples with Gazzi-Dickinson point-counting method (Gazzi, 1966; Ingersoll et al., 1984). Petrographic observations allow the characterization of the main mineralogical components; moreover, heavy minerals have been investigated to highlight abundance and mineralogy. The petrographic investigations were used to identify six petrofacies (PF1 to PF6) in the studied stratigraphic section (Table S2).

4. Facies analysis

Facies analysis of the stratigraphic units and sandstone quantitative point-counting data are reported below, including the description and interpretation of six stratigraphic-depositional units. Each stratigraphic-depositional unit is characterized by different facies association (FA) assemblages (Table 1). Labels between brackets are those here used, whereas detailed descriptions and interpretations of the respective lithostratigraphic unit are reported in the text.

4.1. *Weller Coal Measures (Unit A - sandstone-coal depositional unit)*

4.1.1. *Description*

This unit, at least 70 m thick and corresponding to the Member C of the Weller Coal Measures (Ballance, 1977), is dominated by the alternance of sandstone and coal beds. This unit is featured by FA CCS (carbonaceous-rich cross-bedded sandstones) and FA CCF (coal and carbonaceous mudstones). Sandstones and coal-carbonaceous bodies show mainly sheet geometry and they maintain constant thickness for at least a few kilometers (Fig. 5A). Internally, FA CCS consists of very fine to coarse-grained sandstones dominated by trough cross-bedding organized in multistorey bedsets up to 8 m thick, interlayered with levels of carbonaceous mudstones and coals of FA CCF (Fig. 5C). The FA CCS body in the middle of the unit shows coarser grain-sizes up to trough cross-bedded pebbly sandstones.

FA CCF levels are 1 to 12 m thick and consist of a close association of laminated mudstones, carbonaceous mudstones, and coal horizons. Coal seams, up to 3.5 m thick, are interbedded within carbonaceous mudstone or directly overlain by sandstone bodies through sharp contacts, marked by load and erosional injection structures. The laminated and carbonaceous mudstones are rich in *Glossopteris* leaf impressions and root traces (Fig. 5B); non-arborescent Equisetales taxa have been recorded (Tewari et al., 2015). A great diversity of glossopterids has been revealed for the whole Permian of Antarctica, including Allan Hills (Retallack et al., 2005; Decombeix et al., 2012; Gulbranson et al., 2012, 2014; Tewari et al., 2015). *Gangamopteris* as well and *Vertebraria* roots have been also recorded (Retallack et al., 2005; Decombeix et al., 2009, 2012; Gulbranson et al., 2020). Heterolithic sandstone/carbonaceous siltstone partings are also present particularly in the upper part of the unit, giving rise to a rhythmical alternation and lamination. Peat remnants and fossil trees occur as current-transported and locally *in situ* within FA CCF deposits. In the uppermost thick coal bed, marking the top of this stratigraphic unit, elongated inertinite has been recorded within the organic matter (Corti, 2021).

Petrographic analysis of the sandstones shows a compositional homogeneity throughout Unit A, which is characterized by the petrofacies PF1 (Table S2). The mineralogical composition allows classification of the sandstones as arkose and sub-arkose (Fig. 6). Heavy minerals, mainly garnet, tourmaline, zircon, rutile, and titanite are abundant within PF1.

The passage to the overlying Unit B (Feather Conglomerate) is characterized by an intermediate interval with peculiar lithological features ("transitional interval").

4.1.2. *Interpretation*

Sandstone bodies of FA CCS represent in-channel deposits (*sensu* Miall, 2006), formed by sandy bedforms (SB) and downstream- and lateral-accretion macroforms (DA and LA respectively; see also in Gulbranson et al., 2020). The heterolithic sandstone-carbonaceous siltstone interval testifies for pulsating energy discharge, that could be related with seasonal variability (Fielding et al., 2018). The coarser gravel facies body in the middle of the unit indicates a phase of increasing water discharge and sediment supply, without paleoflow change, likely related to tectonic uplift and/or paleoenvironmental changes (Fielding et al., 2021). Mudstone deposits of the FA CCF are organized in overbank fines (OF) that mean sedimentation both as floodplain and levée deposits in a lowland alluvial plain (Miall, 2006; Fielding et al., 2021) where swamps formed. The occurrence of abundant fossil vegetation, as well as *in situ* trees, indicates a rich-vegetated floodplain crossed by channels delimited by levée. The few thin sandstone beds, with sharp base, interlayered with mudstones are characteristic of crevasse splay setting, due to overbank flooding from the close fluvial channel (Burns et al., 2019). The close association between mudstone, carbonaceous mudstone, and coal of the FA CCF suggests variability in paleowater table position across the shallow standing water mires with different clastic and vegetation influx in the floodplain, preventing or favoring the coal development. The occurrence of permineralized peat and of Histosol agrees with a wetland ecosystem characterizing the alluvial plain (Gulbranson et al., 2020).

The resulting fluvial style for the Unit A is probably a moderate- to low-sinuosity stream system with significant channel stability and high-grade forested floodplain (Isbell and Cúneo, 1996) and in-channel islands, as *in situ* fossil stumps on sandstone macroforms indicate (Gulbranson et al., 2020). The environment can be schematized with a fluvial style intermediate between sandy meandering to anastomosed, with stable backswamp areas. The stabilization of the streams may be induced also by the dense vegetation (Cùneo et al., 1993). The rhythmically interlaminated siltstone-sandstone couplets can infer slight tidal influence on the fluvial system (Dalrymple, 1992), so the environment can be hypothesized as a fluvially-dominated tidally modulated to influenced river system (after Plink-Björklund, 2005 and Gugliotta et al., 2016).

4.2. *"Transitional interval"*

4.2.1. *Description*

This interval, even if it looks like the Weller Coal Measures, shows lithological and compositional transitional features between Unit A and Unit B; it is subdivided into 4 subunits (a to d from the bottom) on the

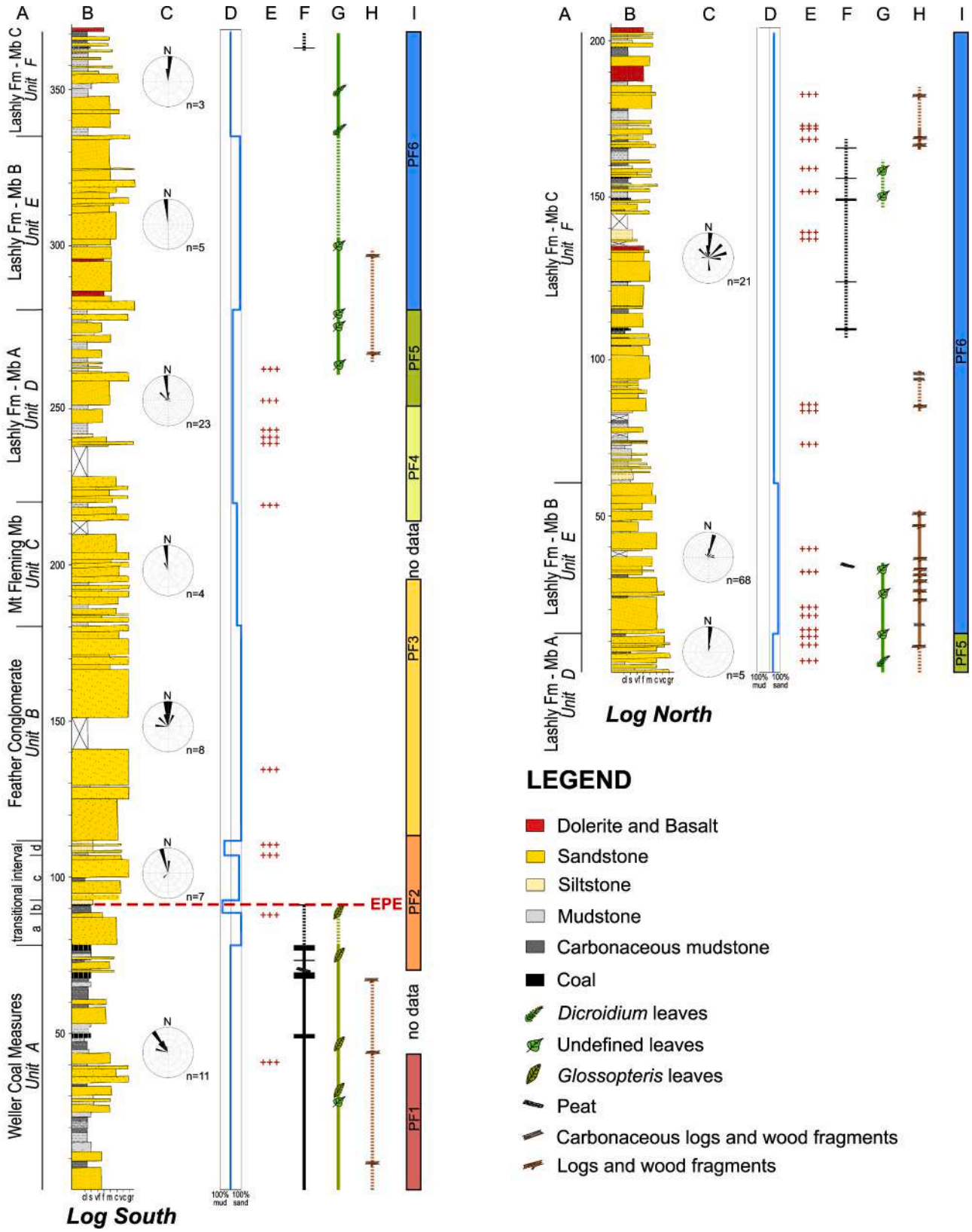

Fig. 4. Synthetic composite stratigraphic logs of the studied sequences of Allan Hills; section traces of the logs are reported in Fig. 3. A) Lithostratigraphic units and depositional/stratigraphic units and sub-units; B) stratigraphic log; C) main paleocurrent directions with respect to the North. The number of measures is reported; D) sand/mud ratio; E) paleosols and oxidized layers; F) coal abundance and occurrence; G) leaf impressions/compressions occurrence and abundance; H) fossil wood fragment and log occurrence and abundance; I) petrofacies based on sandstone composition. Petrofacies description is in Table S2. Continuous line indicates common occurrence; dashed line indicates rare occurrence. EPE: end-Permian extinction; cl: claystone; s: siltstone; vf: very fine sandstone; f: fine sandstone; m: medium sandstone; c: coarse sandstone; vc: very coarse sandstone; gr: gravel.

Table 1
Description of the Facies Associations (FA). Sedimentary facies scheme is shown in Table S1. Facies and architectural elements follow Miall, 1996, 2006. DA: downstream accretion; LA: lateral accretion; GB: gravel bedform; OF: overbank fines; SB: sandy bedform. The depositional units and subunits where facies associations occur are shown. Ta: subunit a of the "transitional interval"; Tb: subunit b of the "transitional interval"; Tc: subunit c of the "transitional interval"; Td: subunit d of the "transitional interval".

Facies Association	Code	Facies	Description	Elements	Units
Cross-bedded pebbly sandstones	PBS	St, Sp, Ss, Se, Gt	Coarse-grained to pebbly sandstone and microgravel beds some meters thick with erosional to amalgamation bottom surface. Trough cross-bedding with rare ripple cross-lamination on top. Plane-parallel bedding and lamination occur in few sandstone beds. Pebble lags and mud clasts. Mineral paleosols (in Unit B and subunit c). Root traces. Carbonaceous and woody fragments occurs in Unit D.	LA-DA-GB-SB	Tc-B-C-D
Carbonaceous rich cross-bedded sandstones	CCS	St, Sl, Sp, Ss, Se, Sr, rare Gp, Gt, Gm	Very fine to coarse-grained sandstone bodies up to some meters thick. Trough cross-bedding with ripples on top and major bedding surface inclined relative to paleo-flow. Heterolithic stratification. Woody debris (WD). Carbonaceous thin wavy laminae and film alternated with sandstone. Local erosional surfaces, scours, rare mud clasts. Locally, planar cross-bedding. Basal pebble lag occur in bedsets. Slight bioturbation may be present (only in Unit A). Reddish sandstone crusts occur.	LA-DA-SB	A-Ta
Cross-bedded sandstones	CBS	St, Sr, Se, Sh, Sr, Sp	Fine to coarse-grained sandstone beds up to some meters thick, with interlayered rare pebbly sandstone beds. Erosional base of the beds forming minor channel and scour, with small dune-scale cross bedding preserved at the top. Trough cross-bedding, ripple cross-lamination, Rare planar cross-stratification and fluid-escape deforming-structures. Peat raft and Large Woody Debris (LWD) with silicified to carbonaceous drifted trunks embedded in the sandstone bodies (in Unit E). Mud clasts Hummocky-like structures may occur. Massive sandstone beds with ripples and wavy lamination forming heterolithic stratification (Unit F). Occasional massive microgravel beds are present with erosional base, mud clasts and rare normal to reverse grading. Bioturbation.	DA-LA-SB	D-*E*-F
Coal and carbonaceous mudstones	CCF	Fsc, Fl, Fsm, Fr, C	Tabular beds of usually carbonaceous shale to siltstone, rich of woody debris and leaves impression. Flat to ripple cross-lamination, rhythmic lamination; heterolithic stratification in tabular beds of carbonaceous siltstone/fine sandstone. Histosols. Roots bioturbation. Peat remnants. Tabular coal beds with lenticular sandstone or siltstone interlayers.	OF	A-F
Carbonaceous mudstones	CBF	Fsc, Fl, Sh	Dark grey to black carbonaceous shale and siltstone tabular. Plane-parallel and ripple cross-lamination. Leaf compression. Presence of nodules and charcoal fragments (subunit b); carbonaceous laminae and mud clasts. Ripple fine-grained sandstone bed occurs at the base of the mudstone horizon and massive fine-grained thin sandstone bed interlayered with mudstone.	OF	Tb-E
Laminated mudstones and fine sandstones	LAFS	Fsm, Sh, St, Sm	Plane-parallel to ripple cross-laminated grey mudstones to very fine sandstones tabular beds up to 1.5 m thick. Trough cross-bedded medium-fine grained sandstone beds; massive dark greywacke on top. Presence of brecciated shale.	OF	Td
Laminated mudstones	LAF	Fl, Fr	Plane-parallel to ripple cross-laminated or minor massive grey mudstones in tabular beds. Rare trough cross-bedded sandstones may occur interlayered within mudstones. Root traces and bioturbation may occur. Leaf compressions in Unit D. Argillosols.	OF	C-D

basis of lithological and sedimentological features. Its lower limit corresponds to the top of the uppermost thick coal seam (ca. 2 m thick) of Unit A, while the upper boundary corresponds to the top of a dark greywacke bed. Detailed sedimentological logs recording the "transitional interval" are shown in Fig. 7.

The "transitional interval" is characterized by the occurrence of a mix of facies associations recurring in the two vertically bounding units (units A and B): the FA CCS (carbonaceous-rich cross-bedded sandstones), characterizing subunit a and recurring within Unit A, and the FA PBS (cross-bedded pebbly sandstones) characterizing the subunit c and forming the Unit B. Fine deposits of the FA CBF (carbonaceous mudstones), resembling those of Unit A, characterize the subunit b, whilst those of the FA LAFS (laminated mudstones and fine sandstones) characterize the subunit d.

The ca. 10 m thick "subunit a – sandstone with carbonaceous content" is dominated by FA CCS and occurs as a sandstone sheet conformably overlying the uppermost very thick coal bed of the Unit A (Fig. 5D). A lenticular coal bed occurs in the lowest part of the sandstone horizon, while coal streaks and carbonaceous laminae are diffused through the sandstone, and decrease upwards. Two meters up from the bottom, thin red ferruginous horizons occur within sandstone strata. Paleocurrents from cross-bedding mainly show NNW flow directions (Fig. 7).

The "subunit b – carbonaceous mudstone", 4.5 m thick, is constituted by FA CBF. A reddish ferruginous sandstone horizon marks the base of subunit b (Fig. 5E); it was previously ascribed as evidence of a potentially unconformable boundary between the Weller Coal Measures and the Feather Conglomerate (Collinson et al., 1983). However, no significant erosional features occur, and its geometry is laterally continuous at least for some kilometers. The top of the reddish sandstone body has been called bounding surface S1 (Fig. 7). Above, a carbonaceous mudstone containing charcoal fragments and leaf impressions/compressions occurs (Figs. 7, 8); fossil leaf associations only include *Glossopteris*, all other leaves are poorly defined. This is overlain by thinly laminated and fissile mudstone containing amorphous organic matter. The mudstone passes upwards to a 1.5 m thick coal-shale and plane-parallel to gently undulate laminated black to grey carbonaceous silty mudstone including lenses of soft-deformed fine sandstone with carbonaceous wispy laminae (Fig. 8); in the lower part of this interval, a thin (ca. 20 cm thick) coal bed occurs (Figs. 7, 8). The top siltstone layer, characterized also by soft-deformed chaotic texture, contains thin coarse sandstone interlayers forming yellowish to grey-green nodules and concretions; within the sandstone matrix, abundant small (ca. 10 μm) crystals of jarosite occur (Fig. 8).

The "subunit c – sandstone with nodules" is 14 m thick and it is marked at the base by very coarse sandstones with trough and tabular cross-stratification and diffuse yellowish to grey-greenish nodules referable to the FA PBS (Fig. 8). At the base, the very coarse-pebbly sandstones show minor erosional features, expressed as scours and impact-injection structures on the underlying mudstone-siltstone level of the top of the "subunit b" (Fig. 8). These basal sandstones contain dark and grey mudstone clasts, remnants of mudstone beds, and alternates between pebbly sandstone and mudstone beds. Internal erosional features define discontinuous mudstone beds and chaotic sandstone-mudstone horizons are also present in the lower part of the subunit. Above, carbonaceous mudstone levels are interlayered. Upwards the FA PBS of the "subunit c" shows an increase in coarse-sized sand with trough cross-bedded very coarse to pebbly sandstones with granule

quartz clasts, lacking any carbonaceous interlayer or film, with a reddish oxidized fine sandstone and few carbonaceous nodules/concretions at the top (Fig. 7). Rare root traces and bioturbations are present at the top of the subunit c. Paleocurrent directions change from NNW to main N direction, however with significant dispersion also to NW (Fig. 7).

The "subunit d – siltstone and oxidized sandstone" is 3.5 m thick and it is formed by the FA LAFS. It is represented at the bottom by a faintly brecciated and mottled grey mudstone lying on a wide surface marked by an oxidized reddish sandstone horizon, marking a major bounding surface (S2). The faintly brecciated mudstone is laterally discontinuous and shows a chaotic texture, containing also mottled structures in its upper part (Fig. 5F). It is overlain by a 0.5 m thick, lenticular medium cross-bedded sandstone bed (Fig. 5F). Above, fine to medium sandstone beds show cross-stratification and black nodules. The uppermost part of the "subunit d" is marked by a 1.5 m thick, dark grey, matrix-rich sandstone bed. From a textural point of view, it is considered as a greywacke, due to the significant amount of muddy matrix. The surface S3 marks the boundary between the subunit d and the Unit B, corresponding to a slight erosional surface juxtaposing cross-bedded sandstones with yellowish altered colour and concretions onto the dark greywacke bed.

Compositionally, sandstones of the "transitional interval" are represented by PF2 (Table S2); broadly, a general trend of quartz increase and feldspars decrease upwards (from subunit a to d) is observable. Compositionally, the sandstones are quartzarenite to subarkose (Fig. 6), but with a general reduction of feldspars content compared to Unit A and the disappearance of plagioclase; however, the feldspars/quartz ratio is higher than those of Unit B. Moreover, the interlayering of strata with composition resembling those of Unit A and of Unit B strengthens the categorization of this as a transitional interval. The heavy mineral assemblage of PF2 is similar to those of PF1, whereas titanite is rare. An upward reduction of garnet abundance, coupled with an increase of tourmaline grains is observable; in general, the total amount of heavy minerals is lower than that of PF1.

4.2.2. Interpretation

The FA CCS and the FA CBF, characterizing the subunits a and b respectively, are interpreted as referable to in-channel sandy deposits (LA and DA macroforms and SB), and as OF respectively. The high-concentration of carbonaceous mudstone implies settlement in back-swamps and ponds in the floodplain, but with high fluvial clastic input, inhibiting the formation of coal. These observations support an interpretation of a moderate- to low-sinuosity sandy bed river with vegetated floodplain for the subunits a and b. Furthermore, the lack of bioturbation and the fissile mudstone in the FA CBF could signify a dysoxic to anoxic pond environment (Fielding et al., 2021) with wildfires testified by charcoal fragments. The uppermost coal-carbonaceous bed, which lies above the last *Glossopteris* leaves, marks the terrestrial EPE. The uppermost part of the subunit b shows strong analogies with the Frazer Beach Member (McLoughlin et al., 2021) and the other Permian-Triassic sequences of the Sydney Basin (Fielding et al., 2019, 2021; Vajda et al., 2020).

The subunits c and d are characterized by FA PBS for in-channel sand bodies (DA macroforms and SB) and FA LAFS for OF respectively. The coarse grain size and the facies of the FA PBS suggest a high-energy stream as a sandy braided stream in a poorly vegetated alluvial plain, with upwards gradual increasing detrital discharge as facies and CU trend seem to indicate. The FA LAFS shows features typical of fine sedimentation in a not vegetated or poorly vegetated floodplain with frequent overbank clastic discharge.

Based on the facies associations, the "transitional interval", differently from the coeval units of the Sydney Basin (Fielding et al., 2021), marks a gradually changing fluvial style from Unit A to the overlying Unit B. The subunits a and b, showing features comparable with those of Unit A, are related to a moderate- to low-sinuosity fluvial style with more or less wide floodplain with marshes. Differently, the subunits c and d, having features more similar to the Unit B, are referable to a low-sinuosity sandy-gravel braided fluvial system. This evidence emphasizes the changing fluvial style and the increase in energy and clastic-discharge across the "transitional interval". Paleocurrents are consistent with a slight change in fluvial direction, from NW to NNW, which can be also imputed to a moderate avulsion linked with the change in the fluvial regime.

4.3. Feather Conglomerate (Unit B - pebbly sandstone depositional unit)

4.3.1. Description

Unit B, ca. 80 m thick, is characterized by sandstone beds of the FA PBS (cross-bedded pebbly sandstones) and the lack of coal or carbonaceous interlayers and fragments, with very rare mudstone interbeds (Fig. 4). The FA PBS consists of whitish coarse-grained to microgravel and pebbly sandstone beds with erosional to amalgamated bottom surface; red oxidized patina and encrusting surfaces are common (Fig. 9A). Trough cross-bedding grades to ripple cross-lamination on top of a few coarse-grained beds; plane-parallel bedding and lamination occur in few sandstone beds. Weakly developed paleosols (Protosol) occur (Gulbranson et al., 2020), as well as vertical burrows in the lower part (Barrett and Fitzgerald, 1985; Fitzgerald and Barrett, 1986).

The pebbly sandstone bodies form a coarsening upward trend (CU), coupled with a slight change in paleocurrents towards N in the lower part, to mainly NW in the upper part (Fig. 4).

The stratigraphic boundary delimiting the units B and C is conformable, marked by a gradual reduction in sandstone grain-size and bed thickness, and by the upwards appearance of mudstone interbeds with a different architectural stacking pattern. The sandstone beds acquire a most evident stratification and tabular geometry.

The pebbly sandstones composition of the Unit B resembles the PF3 (Table S2). Based on mineralogical composition, PF3 sandstones are quartzarenite to quartz-rich sub-arkose (Fig. 6). PF3 is also characterized by a low number of heavy minerals, mainly represented by tourmaline, zircon, and rutile; garnet is rare within this petrofacies.

4.3.2. Interpretation

Pebbly sandstones of the FA PBS are interpreted as coarse channel fills of a low-sinuosity river. The cross-bedded macroforms correspond to DA and gravel to sandy bedforms (GB and SB; *sensu* Miall, 2006) within a high-energy braided low-sinuosity fluvial system, where the flooded alluvial plain was narrow in width. The lack of an alluvial plain with overbank deposits, as well as riparian vegetation, is suggested by the absence of fine deposits, mud clasts, and vegetation remnants. The CU trend testifies to an increase of landscape gradient accompanied by a reduction of vegetation in response to global-scale climate change as stated by Collinson et al. (2006), and to a probable contribution of the backland tectonic uplift (Collinson et al., 1994). Conversely, the uppermost FU sequence testifies for a progressive reduction in clastic discharge with the forming of a broader floodplain.

The fluvial style for this unit is interpreted as a perennial gravel- to sand-bed braided river (Miall, 1978, 2006; Barrett and Fitzgerald, 1985).

4.4. Mt. Fleming Member (Unit C – coarse sandstone-mudstone depositional unit)

4.4.1. Description

This unit, ca. 30–40 m thick, corresponds to the Mt. Fleming Mb. of the Feather Conglomerate, (Barrett et al., 1971; Collinson et al., 1983, 1994), and it shows a different stacking pattern compared to Unit B (Fig. 4).

Unit C is composed by FA PBS (cross-bedded pebbly sandstones) and FA LAF (laminated mudstones). FA PBS consists of whitish coarse-grained sandstone to microgravel beds with erosional to amalgamated bottom surface; trough cross bedding and ripple lamination are

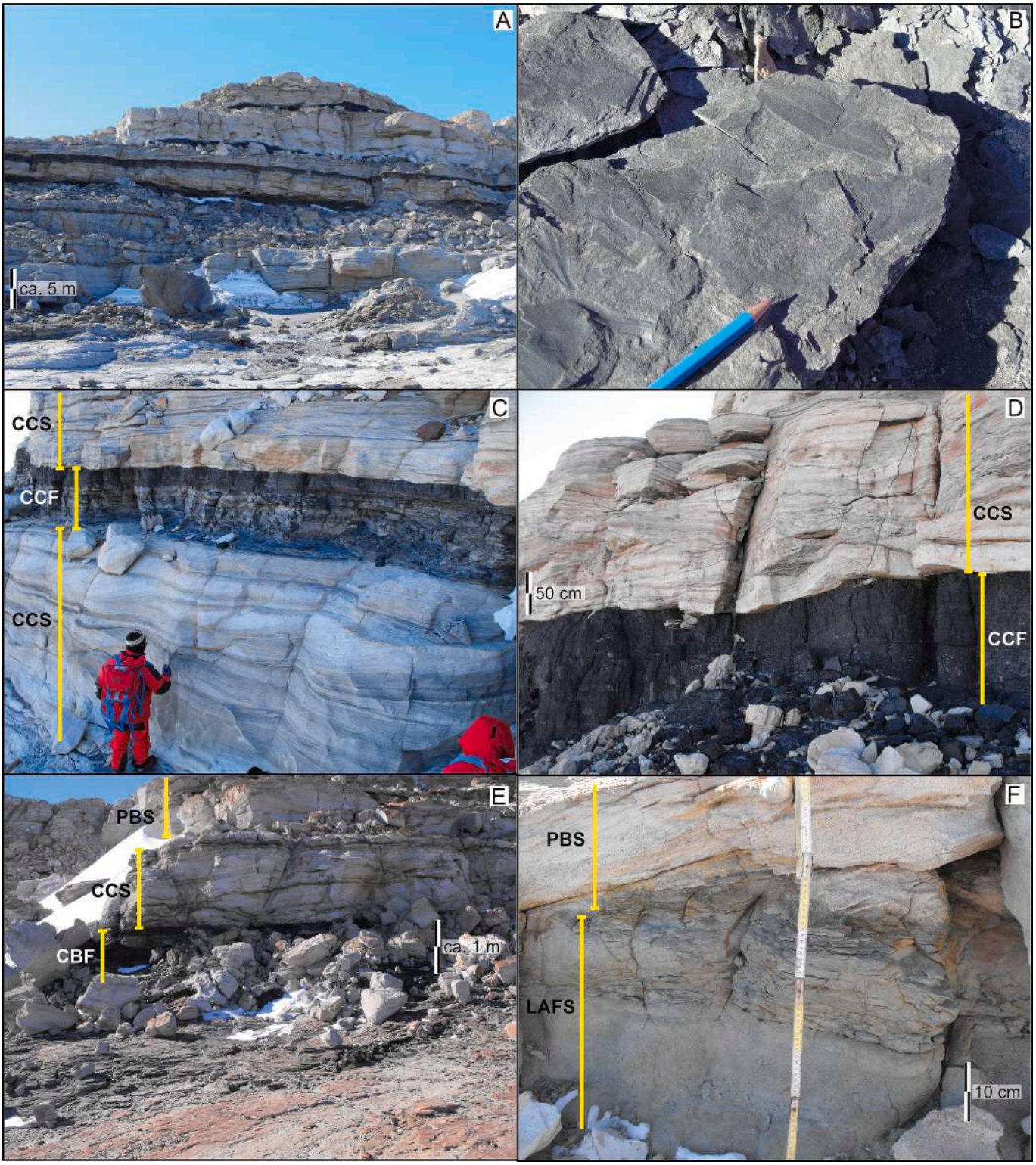

Fig. 5. Field photographs of the Unit A (Weller Coal Measures) and "transitional interval". Facies associations are shown; their description is provided in Table 1. A) Alternation of coal and carbonaceous mudstone layers (dark) with sandstone beds (grey); B) *Glossopteris* leaf impressions/compressions within FA CCF; C) detail of coal seam between two sandstone beds with carbonaceous laminae; D) trough cross-bedded sandstone at the base of the subunit a above the uppermost Unit A coal seam; E) large view of the subunit b and passage to subunit c (grey sandstones). Red encrusted bed at the base represents the surface S1; F) detail of the faintly brecciated and mottled mudstone at the base of subunit d. (For interpretation of the references to colour in this figure legend, the reader is referred to the web version of this article.)

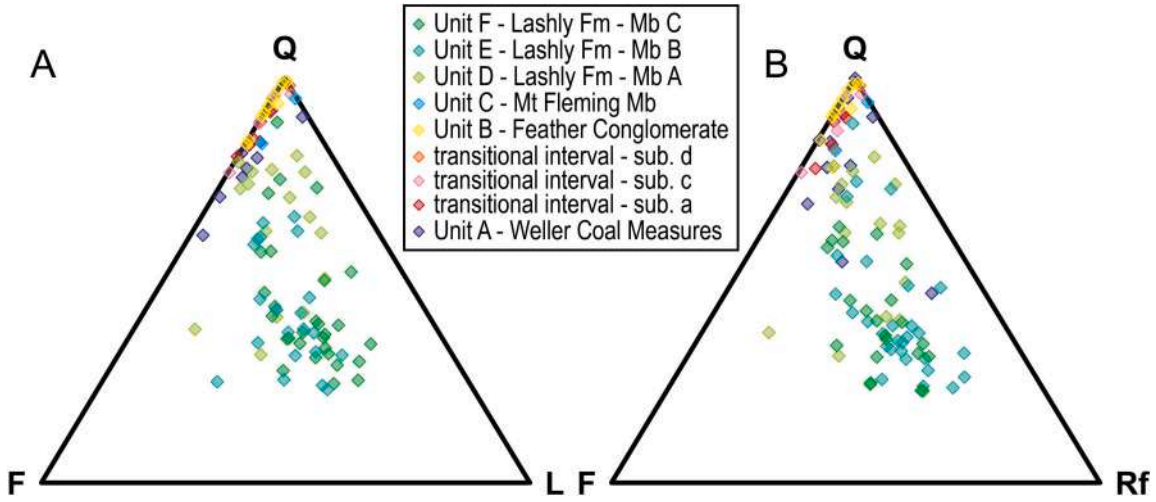

Fig. 6. Ternary diagrams of the sandstone composition of each unit. Point-counting was carried out with the Gazzi-Dickinson method (Gazzi, 1966; Ingersoll et al., 1984). A) Ternary diagram following Dickinson (1985) and Garzanti (2019). Q: quartz (monocrystalline, coarse polycrystalline and quartz in coarse grained lithic fragment); F: feldspars (monocrystalline and feldspars in coarse grained lithic fragments); L: lithic fragments (fine grained polycrystalline quartz and lithic fragments); B) ternary diagram following (McBride, 1963). Q: quartz (monocrystalline and polycrystalline); F: feldspars (monocrystalline); Rf: rock fragments (quartz and feldspars in lithics and lithic fragments).

common, while plane parallel bedding and lamination are rare (Fig. 9B). The occurrence of FA LAF marks the main difference with the underlying Unit B. The LAF deposits form horizons 0.70 to 1.5 m thick, with the thickest one marking the contact with the overlying Unit D. This last bed represents a well-developed mottled paleosol with chaotic structure. The sandstone and particularly the pebbly sandstone facies are characterized by significant concentrations of mud clasts and, in the upper part, by large detrital white mica crystals aligned in laminae.

Paleocurrents measured in the trough cross bedding indicate flows mainly towards NNW (Fig. 4).

Even though the low number of analyzed samples, sandstones of Unit C present different compositions. The lowermost part of Unit C closely resembles petrofacies PF3, while the middle-upper portion resembles PF4 (Fig. 4). Heavy mineral assemblage closely resembles those of PF3 (Table S2).

4.4.2. Interpretation

The FA PBS deposits are organized to form SB and GB, and DA macroforms (Miall, 2006); the FA LAF deposits represent OF (Miall, 2006). These are consistent with a fluvial system maintaining a high energy, but relatively less than that for the Unit B. This slight reduction in inferred stream power is consistent with the development and widening of the floodplain; this is testified by the laminated mudstone partitions, the enrichment in bioturbation, and the presence of mud clasts within the pebbly sandstone bodies. This last unit documents the high energy and erosional capabilities of the gravel-sand flows, reworking the fines of the alluvial plain, where they were constrained during the major flooding events. Paleosols observed within this unit are similar to Lower Triassic ones described in the overlying Lashly Fm. (Retallack and Krull, 1999; Gulbranson et al., 2020). The paleosol at the boundary between units B and C is an Argillisol showing alternating reducing and oxidizing environmental conditions (Gulbranson et al., 2020).

The resulting fluvial style is interpreted as a perennial gravel- to sand-bed braided river, but with minor energy and formation of a vegetated alluvial plain, also related to the recovery of climate conditions (Retallack and Krull, 1999).

4.5. Lashly Fm. Member A - (Unit D - medium-fine sandstone-mudstone depositional unit)

4.5.1. Description

This unit, ca. 60 m thick, is distinguished from the underlying Unit C by a different stacking pattern (Fig. 4), due to the increase of mudstone interbedded with coarse-gravelly sandstones, and by a higher sandstone/mudstone ratio (≥ 1). Unit D could be considered the Member A of the Lashly Fm. as described by Barrett and Kohn (1975) and Collinson et al. (1983), occurring in Log South and partially in Log North (Fig. 4).

The unit D is characterized by an assemblage of three facies associations (Fig. 9): the FA CBS (cross-bedded sandstones), the FA PBS (cross-bedded pebbly sandstones), and the FA LAF (laminated mudstones). The FA CBS, characterized by fine to coarse grained trough cross-bedded sandstones, is the most abundant. However, heterolithic sandstone-mudstone partitions also occur. FA PBS, dominated by massive or trough cross-bedded strata, is subordinated. Carbonaceous fragments, coal and woody debris (WD), and mud clasts are encased within gravelly beds with chaotic structure. Mudstone interlayers, up to 3.5 m thick, of the FA LAF occur. Mudstones often show paleosol features and bioturbation; paleosols are Protosols and Argillisols (Gulbranson et al., 2020). *Dicroidium-Heidiphyllum* leaf compressions are present in the upper part of the unit, including three *Dicroidium* species (Escapa et al., 2011), as well as *in situ* tree stumps. Furthermore, thalloid macroalgae fossils were recovered by Bomfleur et al. (2009), as well as *Neocalamites* compressions (Gulbranson et al., 2020).

Paleocurrent data from foresets of the sandstones show a dominance towards NNW with minor dispersion towards W to E in the Log South, and NNE in the Log North (Fig. 4). The general stacking pattern shows a general reduction of bed thickness and grain-size with respect to Unit C.

Compositionally, the lowermost sample of this unit resembles PF4; on the contrary, most of the sandstone samples have a PF5 composition (Fig. 4; Table S2). The lithic fragments of the PF5 are mainly represented by felsic volcanic and sub-volcanic rocks, and minorly by intermediate to mafic volcanic ones. PF5 sandstones are classified as feldspathic litharenite and lithic sub-arkose (Fig. 6). Heavy minerals are not abundant, and the assemblage is made up of zircon, garnet, titanite, tourmaline, rutile, and apatite.

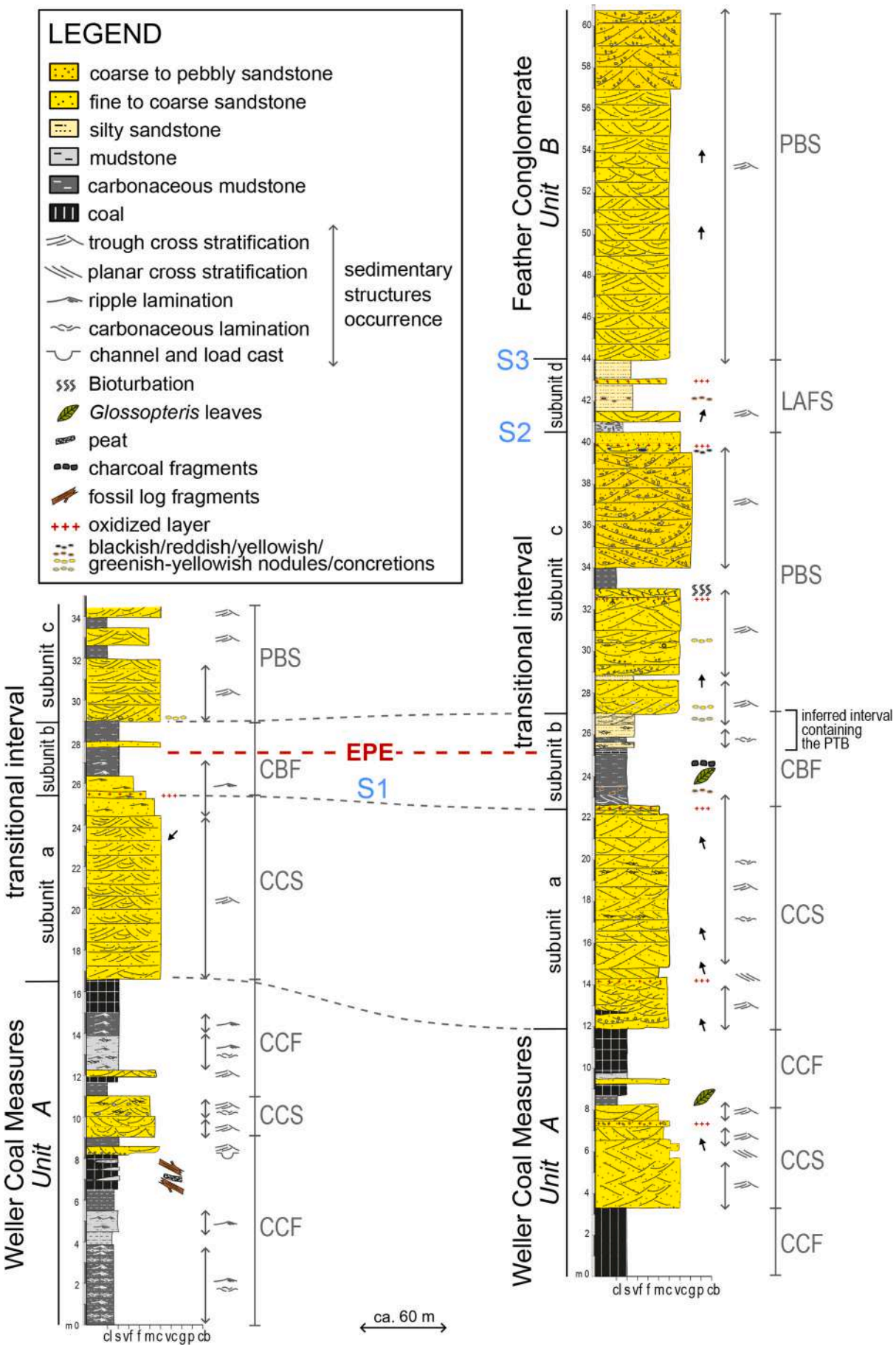

(caption on next page)

Fig. 7. Detailed sedimentological logs of the "transitional interval" from two sections: log traces are shown in Fig. 3. Subunits of the "transitional interval" and Units, as well as bounding surfaces, are reported and correlated. Facies association are shown; their description is provided in Table 1. The end-Permian extinction (EPE) is placed above the last thin lenticular coal bed. PTB: Permian-Triassic boundary; cl: claystone; s: siltstone; vf: very fine sandstone; f: fine sandstone; m: medium sandstone; c: coarse sandstone; vc: very coarse sandstone; g: gravel; p: pebble; cb: cobble.

4.5.2. Interpretation

The FA PBS and CBS resemble in-channel elements, mainly DA macroforms, with minor LA macroforms, SB and GB (*sensu* Miall, 2006). Coarse grained, non-graded, matrix-rich deposits are consistent with chaotic sediment gravity flows (SG; Miall, 1996). The LAF facies association indicates OF elements, which represent floodplain levee deposits (FF and LV elements respectively; Miall, 1996). The moderate dispersion of the paleocurrents suggests a high- to moderate-sinuosity fluvial system, where longitudinal-transversal sand bars and point bars could cohabitate. The occurrence of macroflora-rich mudstones indicates an increase of vegetation, and a less erosion-prone environment, which shows a floristic turnover with respect to the Permian one (Gulbranson et al., 2020). Thus, fossil evidence indicates the re-establishment of rich-riparian vegetation within a wide alluvial plain, where occasional crevasse splays flowed. The occurrence of both bioturbated Protosols and Argillisols indicate a significant mobility and avulsion of the channel within the floodplain (Gulbranson et al., 2020).

The coarser facies of the FA PBS are representative of gravel bar and element (trough cross-bedded facies) and catastrophic flooding event (chaotic matrix-rich facies with tree remnants), which can be related with a particular climate event and/or tectonic uplift pulses (Fielding et al., 1997, 2021). The presence of *in situ* tree stumps and of upper flow regime structures agrees with a variable fluvial discharge, likely due to seasonal changes (Fielding et al., 2018, 2021).

The different paleocurrents between the southern section and the northern section suggest a northward downstream diversion of the fluvial direction, from NNW to N, of a meandering to sandy wandering river within a well-developed lowland alluvial plain (Miall, 2006).

4.6. Lashly Fm. Member B (Unit E - trunk-bearing medium-coarse sandstone depositional unit)

4.6.1. Description

This unit, occurring in both logs S and N, is characterized by the decrease of mudstones (sand/mud ratio >> 1), which rarely interlayer with sandstones towards the top of the unit (Fig. 4). Unit E represents the Member B of the Lashly Fm., and it is ca. 50 m thick; its lower boundary is conformable with Unit D.

Unit E is characterized by two facies associations: the FA CBS (cross-bedded sandstones) and the FA CBF (carbonaceous mudstones). The elements of the FA CBF form few thin and discontinuous layers of carbonaceous mudstones with *Dicroidium* and *Heidiphyllum* leaf impressions and woody fragments. The plan view of the sandstone bodies forming the FA CBS shows the interfering trough cross-bedding and ripple cross-lamination, characterizing downstream accretion forms with small dune-scale cross-bedding on top.

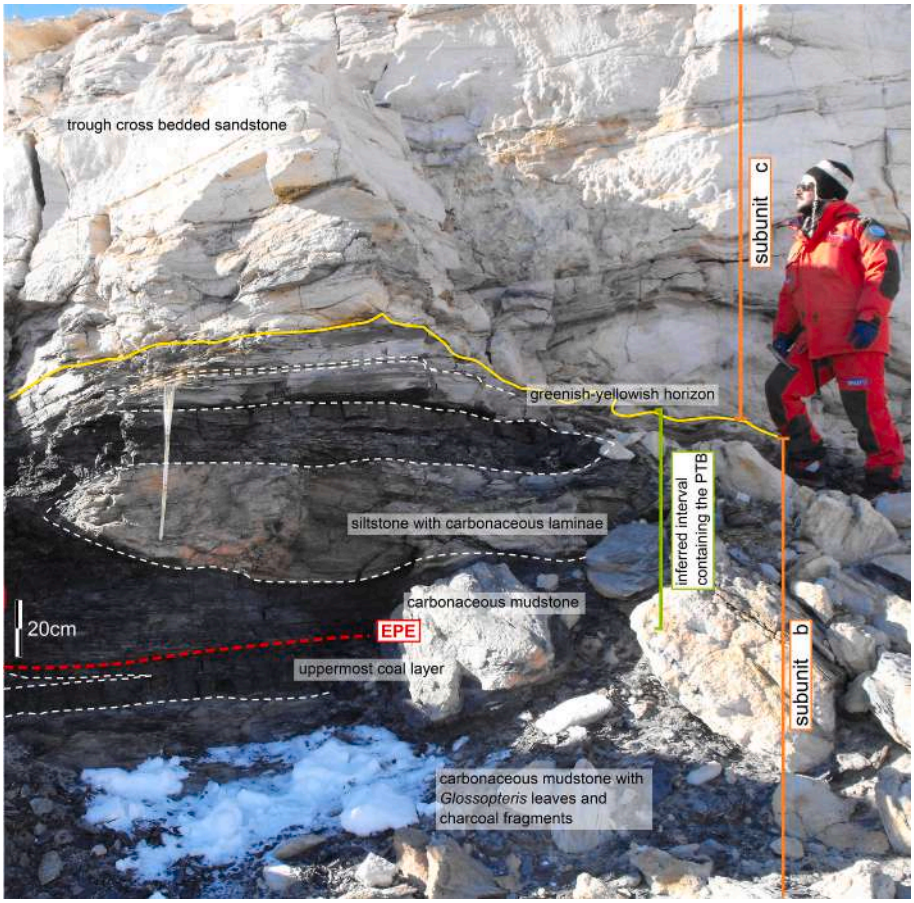

Fig. 8. Field photography of siltstone and carbonaceous mudstone of the upper subunit b and the passage to trough cross-bedded sandstone of the subunit c. The end-Permian Extinction event (EPE) is placed in correspondence with the uppermost coal-carbonaceous bed. The Permian-Triassic boundary is inferred in the interval between EPE and the base of the subunit c. Jarosite-bearing greenish-yellowish layer is shown.

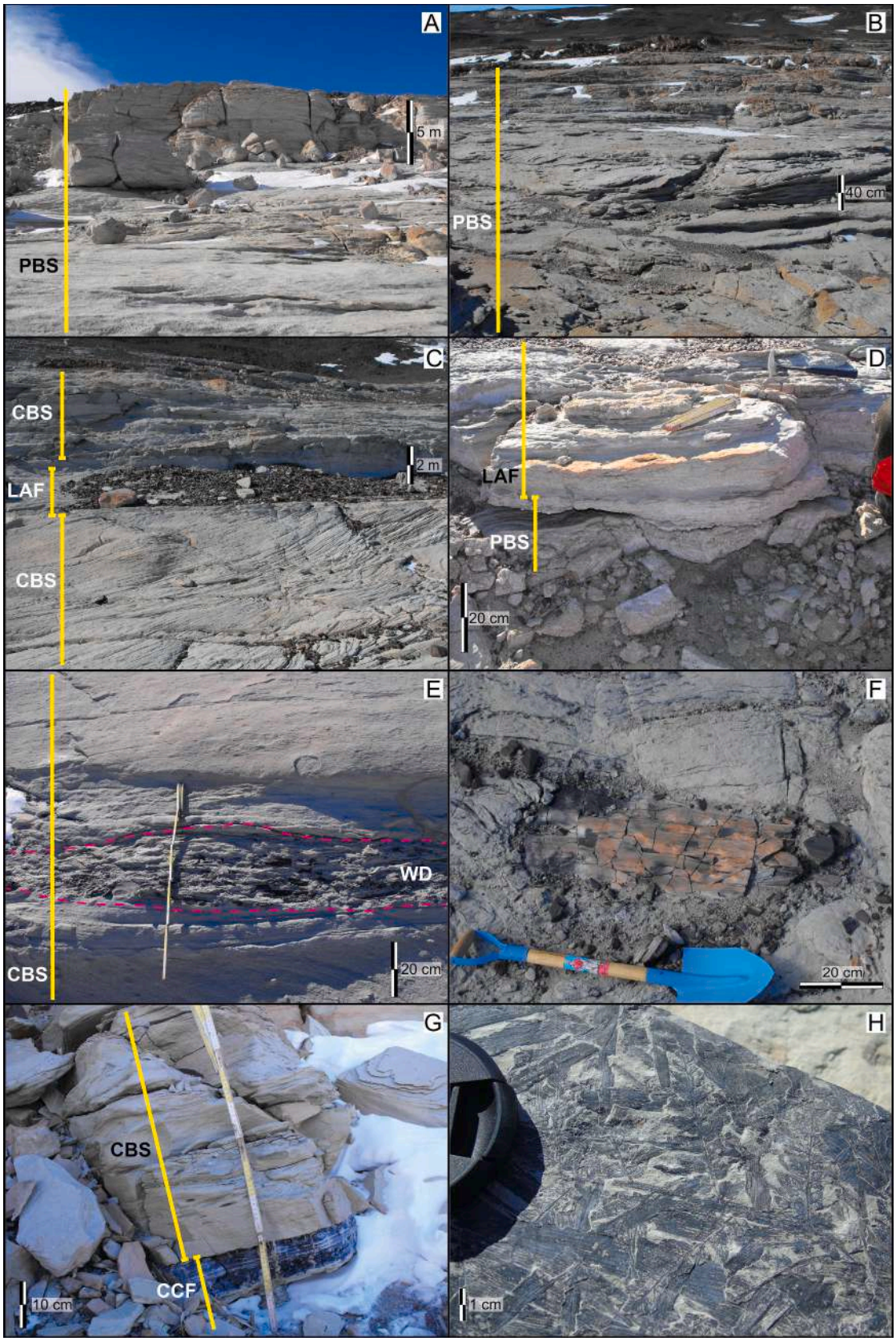

Fig. 9. A) Field photography of the trough cross-bedded coarse sandstones of the Unit B (Feather Conglomerate); B) field photography of sandstones and mudstones of the Unit C (Mt Fleming Member); C—D) field photographs of sandstone and mudstone alternations of the Unit D (Member A of the Lashly Formation); E) field photography of the volcanoclastic sandstone-dominated Unit E (Member B of the Lashly Formation) with a woody debris accumulation; F) silicified trunk within sandstone of the Unit E; G) field photography of the coal and volcanoclastic sandstones of Unit F (Member C of the Lashly Formation); H) *Dicroidium-Heidiphyllum* fossil leaves impression/compression within mudstone layers in the Unit F. Facies associations are shown; their description is provided in Table 1.

The main characteristic of this unit is the occurrence of horizons rich in silicified and partially charcoalified logs and peat rafts as Large Woody Debris (LWD in Gulbranson et al., 2020), encased within sandstone bodies of FA CBS (Fig. 9). Abundant transported fossil wood occurs in the middle part of Unit E (Liberato et al., 2017; Gulbranson et al., 2020, 2022a), in some cases forming logjam concentrations (Gibling et al., 2010; Gulbranson et al., 2020). LWD contain well-preserved permineralized logs, in some cases showing root flare enclosed in the coarse sandstones (Gabites, 1985). The silicified trunks, up to 12–18 m long and 40 cm in diameter, have a high compression ratio (Fig. 9F). A rich floral assemblage characterizes those horizons ("Escapa Heights flora" in Gulbranson et al., 2020), with several species of *Dicroidium*, Ginkgoales, and conifers. *Neocalamites* compressions also occur in fine deposits (Gulbranson et al., 2020).

The lower part of the Unit E shows paleocurrents flowing towards NW in the Log South and mainly NNE with minor dispersion towards ENE in the Log North; the upper part of Unit E in the Log North presents an abrupt paleo-direction change towards ENE (Fig. 4).

The petrofacies PF6 characterizes the sandstone of the Unit E (Table S2). Heavy minerals are common throughout the PF6 and they mainly are zircon, garnet, titanite with rare rutile, apatite, and tourmaline.

4.6.2. Interpretation

Sandstone sheet bodies of the facies association CBS are referred to in-channel deposits forming SB and DA with less LA macroforms (*sensu* Miall, 2006). Carbonaceous mudstones of the facies association CBF are relative to OF (Miall, 2006). The abundance of mud clasts and transported trunks, charcoal, woody debris, and peat raft within FA CBS testifies high-energy discharge events and catastrophic flooding devastating the alluvial plain with its riparian forest and peat bogs (Gulbranson et al., 2020, 2022a). The continuative erosion from the sand floods and the frequent sandstone bed amalgamation results in the thin and rare OF. The pulsating energy of the stream flows is evident from the recurrent interferences through reactivation erosional surfaces, between the high-regime bedforms as DA and 3-D dunes sometimes with pebble lag and debris flows, and low-regime bedforms as ripple-trains and small-dunes. The large blocks of fines encased within sandstones represent a further indicator of the high erosional capability of the floods, able to detach portions of the overbanks. Moreover, paleocurrents show a substantial stability of the stream across the stratigraphic boundary between units D and E for the upstream part of the river (Log South); the downstream part of the river (Log North) shows a progression of the fluvial diversion towards NNE-E, already started with the Unit D.

On the base of the architectural elements and facies associations, the inferred fluvial style for this unit can be seen in a low-sinuosity sandy-braided stream, an intermediate model between the "sheetflood distal sandy-braided" and the "perennial sandy-braided" of Miall, 1985 and Miall, 1996. The fluvial system flowed in a densely vegetated braidplain which also preserves evidence of wildfires (Liberato et al., 2017; Cornamusini et al., 2020) and it was subjected to frequent erosional dismantling of the floodplain (see in Gulbranson et al., 2020, 2022a).

4.7. Lashly Fm. Member C – (Unit F – mudstone-sandstone and coal depositional unit)

4.7.1. Description

Unit F, representing the Member C of the Lashly Fm., at least 130 m thick, is mainly distinguished by the underlying Unit E based on an abrupt reduction of the grain-size and the re-appearance of thin coal layers interbedded with sandstone and mudstone beds (Fig. 4).

Its lower boundary is marked by the appearance of mudstone beds interlayered with sandstones. Two facies associations, the FA CBS (cross-bedded sandstones) and the FA CCF (coal and carbonaceous mudstones) characterize this unit (Fig. 9G). Sandstone bodies of the FA CBS show similar characteristics of the below units D and E, with dominant trough cross-bedding and ripples on top, erosional bottom bed-surfaces, occurrence of mud pebbles and silicified and carbonaceous woody debris. Heterolithic sandstone-mudstone partitions with thin carbonaceous lamination are present. Sandstone bodies show thinning with increase of mudstone bodies frequency and thickness, belonging to the FA CCF, northwards. These are maximum 11 m thick in the Log North, composed of laminated mudstones, carbonaceous mudstone, and thin coal beds (0.5 to 1.2 m thick); lasts occur in the upper part of the unit. Mudstones contain abundant root traces, desiccation cracks, leaf impressions (Fig. 9H), and wood assemblages (mainly *Dicroidium* and *Heidiphyllum, Notophytum*; Escapa et al., 2011), woody debris, and *in situ* fossil stumps (i.e., Roscolyn Tor fossil forest; Gulbranson et al., 2020, 2022a). Thalloid freshwater macroalgae also occur (Bomfleur et al., 2009), as well as fern genera including *Osmunda* and *Taeniopteris* (Townrow, 1967). Paleosols and bioturbation occur throughout. In the Log North, where the Unit F is better exposed, a CU stacking pattern is observable from the bottom to the middle part (Fig. 4); upward a FU stacking pattern occurs.

As for the units D and E, the Log South shows unchanged paleocurrents flowing towards NNW. Differently, in the Log North, as for the underlying stratigraphic units, the paleocurrent directions show significant dispersion, from NE in the lowest part, to E-ESE in the middle part, to NW in the uppermost part (Fig. 4).

The petrographic analysis of the sandstones of Unit F shows that the mineralogical assemblage is referable to that of the PF6 (Table S2).

4.7.2. Interpretation

The facies association CBS is interpreted as multistorey in-channel sandstone bodies where SB, LA and DA macroforms occur within discrete channel belt crossing the alluvial plain (Miall, 2006). This last unit is formed of floodplain deposits characterized by OF, where channel levee fines (LV), floodplain fines (FF), and interlayered sandstone beds of crevasse splay (CS) coexist (Miall, 1996, 2006). Carbonaceous mudstones, coal beds and the abundant fossil plant remains indicate a densely vegetated alluvial plain, with flourishing riparian forests (Gulbranson et al., 2020, 2022a), and backswamps. The abundant clastic drainage inhibited the formation of pure coal bed for the lower part of the unit where carbonaceous mudstones formed; in contrast, the upwards decrease of clastic input allowed the formation of coal bed. The heterolithic partitions with carbonaceous thin layers and mud-sand couplets allow to infer the influence of a slight tidal effect, as revealed for the tidally-influenced/modulated fluvial system model (Plink-Björklund, 2005; Gugliotta et al., 2016).

The resultant fluvial style is interpreted as a moderate- to high-sinuosity sandy meandering stream within a distal alluvial plain characterized by ephemeral backswamps and marshes linked with the fluvial avulsion (Miall, 1996, 2006).

5. Discussion

The facies analysis points out changes in the fluvial style throughout the Victoria Group stratigraphy. The stratigraphic architecture reconstructed in the Allan Hills nunatak by Ballance (1977) emphasized sharp lateral changes. Here, the surface boundaries among the lithostratigraphic units are commonly considered conformable. Nevertheless, minor erosional surfaces are included within the whole succession, but without regional extension (Fig. 10; Retallack and Krull, 1999; Liberato et al., 2017; Gulbranson et al., 2020).

The facies associations characterizing the Unit A (Weller Coal Measures) are consistent with a moderate to low sinuosity stream system. Thus, this depicts the Permian paleoenvironment as a densely vegetated alluvial plain where a sandy meandering to anastomosed river flowed (Fig. 11).

On the contrary, the facies association of the Unit B (Feather Conglomerate), dominated by FA PBS, provides the evidence of the

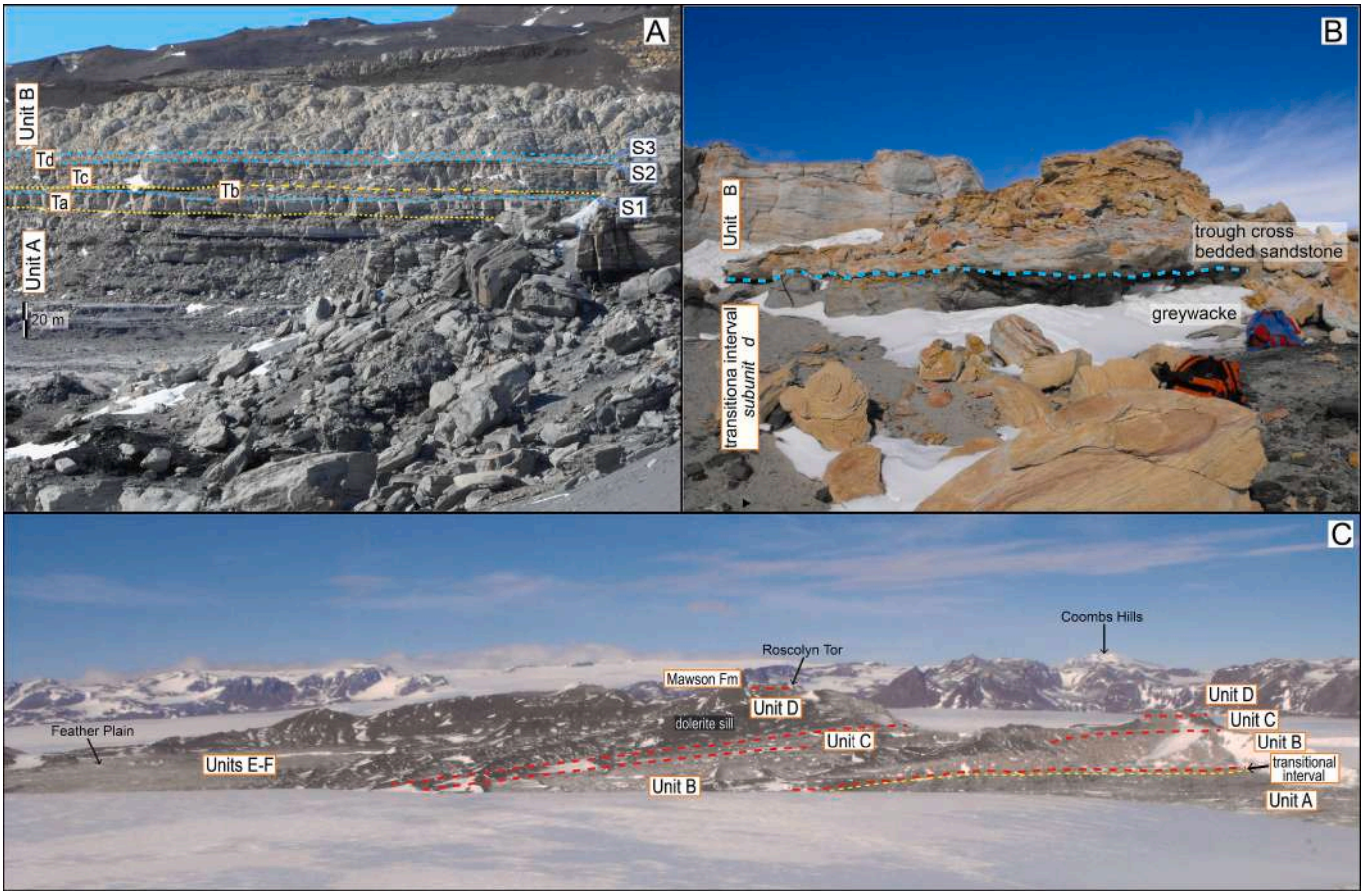

Fig. 10. A) Landscape view of the upper Unit A (Weller Coal Measures), the Unit B (Feather Conglomerate), and the "transitional interval" in between. Ta: subunit a of the "transitional interval"; Tb: subunit b of the "transitional interval"; Tc: subunit c of the "transitional interval"; Td: subunit d of the "transitional interval"; S1-3 are the main bounding surfaces; B) detail of the boundary between subunit d of the "transitional interval" (the upper part of the subunit d consists of a dark greywacke bed) and the trough cross-bedded sandstones of the Unit B (Feather Conglomerate); C) aerial view of the studied portion of Allan Hills with the line drawing of the depositional units.

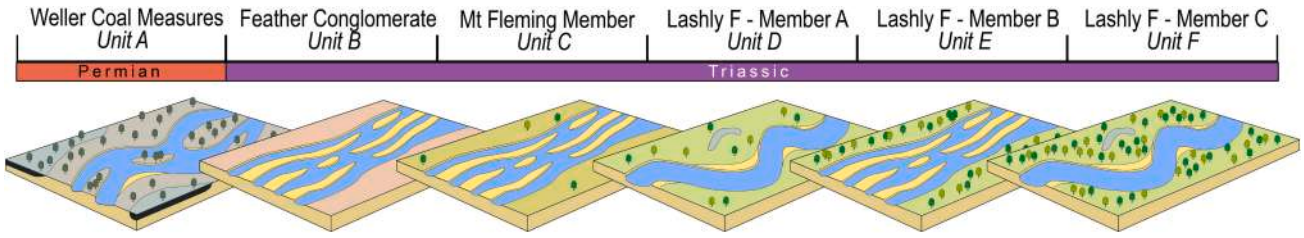

Fig. 11. Schematic evolution of fluvial style through the six depositional-stratigraphic units identified in this study on the base of the facies analysis carried out in the Allan Hills section.

installation of a perennial gravelly to sandy braided river (Fig. 11; Miall, 1978, 2006; Barrett and Fitzgerald, 1985).

Collinson et al. (1983, 1994) observed that the boundary between the Weller Coal Measures and the Feather Conglomerate is marked by an abrupt change in lithology close to ferricrete horizons, suggesting a disconformity also supposed by Isbell and Cúneo (1996). The ferricrete horizons probably do not correspond to paleosols, as they are consistent with supergene diagenetic mineralization. Furthermore, the morphology of iron mineralization in these "ferricretes" is displacive of surrounding sediment and massive, which lacks the nodular or reticulate cementation pattern observed in soil-formed, or supergene, iron mineralization (Kaczorek and Sommer, 2003; Kaczorek et al., 2004; Eze et al., 2014) and the inclusion of soil material in these types of soil-formed iron precipitates. Therefore, these surfaces likely reflect preferential accumulation of iron during diagenesis along bedding plane contacts of sedimentary strata with contrasting hydraulic conductivities.

This study evidences a gradual transition from the facies associations typical of the Unit A (CCS and CCF) to those of the overlying Unit B (PBS), allowing the identification of a "transitional interval". This interval marks a sharp increase of sandstone grain-size, thickness of beds, and the disappearance of coal and mudstone levels, as well as of any wood, leaf, or carbonaceous fragment from the Weller Coal Measures to the Feather Conglomerate.

Furthermore, this transition zone marks the appearance of the Dolores pedotype, commonly occurring in the uppermost Weller Coal Measures and in the Feather Conglomerate (Retallack and Krull, 1999; Retallack et al., 2005; Gulbranson et al., 2020). These paleosols are weakly developed, similarly to the underlying ones in the Weller Coal Measures, but are distinct from the lower paleosols by lacking organic matter accumulations. The occurrence of potential paleosol horizons

within the "transitional interval" represents the development of subaerial surfaces (Retallack and Krull, 1999). As paleosols are abundant in the entire succession, there is a low likelihood that these paleosols reflect, individually, significant gaps in time, but rather lateral shifts in the locus of sediment deposition. Retallack and Krull (1999) and Gulbranson et al. (2022b) indicate that multiple paleosols occur in both units accompanying lateral (Isbell and Cúneo, 1996) and vertical changes in fluvial style. Moreover, the vertical variation in these strata of paleo-discharge and paleoflow direction indicates changes in the water availability to these fluvial systems and the rates of erosion to supply sediment to the depositional basin.

The "transitional interval" also marks a change in paleocurrent flow directions, from NNW (Unit A and subunit a of the "transitional interval") to N and NNE (subunits c and d of the "transitional interval" and Unit B), which is maintained for few tens of m above the interval followed upsection by a change towards mainly NW-W paleoflow direction (units C, D, E, and F).

The petrographic analyses also support the transitional nature of the interval (Fig. 6). The petrofacies PF2 shows an intermediate composition between the PF1, which characterizes the Unit A and where feldspars are common, and the PF3, characterizing the Unit B which is quartz-dominated.

Changes of paleoflow direction, sandstone composition, grain-size and bed thickness could be all explained as due to a marked variation in the pattern and regime of the fluvial system and of the source areas, implied by tectonic and/or climatic variations. However, substantial continuity through the depositional systems of the two units A and B occurs, without emphasize a regional disconformity, in agree with the transitional character of the stacking-bed at the boundary pointed out by the occurrence of a "transitional interval".

Furthermore, the field and aerial observations also indicate the conformable nature of the surfaces delimiting the upper units B, C, D, E, and F. These boundaries are recognizable by changes in the grain size and stacking pattern of the succession (Fig. 10).

The reappearance of OF within the FA PBS of the Unit C, corresponding to the Mt. Fleming Member, points out to an energy decrease of the fluvial system, allowing the preservation of fine sediments in the floodplain (Fig. 11). The decrease of grain size, marked by the disappearance of FA PBS which give place to FA CBS, and the increase of thickness and frequency of fine deposits representing OF, highlight the development of a meandering to sandy-wandering river within a well-developed alluvial plain during the deposition of Unit D, corresponding with the Member A of the Lashly Fm (Fig. 11). Moreover, Unit D records a gradual change in the sandstone composition: from quartzarenite-dominated in units B and C (PF3) to lithic subarkose in the lower Unit D (PF4), up to arkosic lithoarenite-dominated in upper Unit D and units E and F (PF5 and PF6 respectively), which also entails a variation in the sandstone colour. The occurrence of abundant volcanoclastic input in the units D, E, and F sandstones marks a provenance change from a volcanic arc active in the Gondwana margin (Barrett, 1981, 1991; Collinson et al., 1983, 1994); on the contrary, units A, B, and C sandstone composition supports a mainly intrusive and metamorphic basement source.

The Mb B of the Lashly Fm (Unit E) marks an abrupt environmental change, corresponding with the development of a sandy braided river (Fig. 11). The occurrence of fossil log accumulation as LWD indicates a densely vegetated alluvial plain. The sandy braided fluvial style of the Unit E gives way to a sandy meandering fluvial style during the deposition of the Unit F, corresponding to the Mb C of the Lashly Fm (Fig. 11).

The placement of the PTB in the succession of Allan Hills as well as in SVL is controversial. There is a substantial lack of clear paleobiologic evidence in order to correlate these strata with well-defined PTB successions elsewhere. Moreover, there is a lack of U—Pb ages. Thus, the most reasonable data to constrain the position of the PTB in this region are palynomorphs that can be correlated to the U—Pb age-calibrated palynostratigraphy of Eastern Australia (Fielding et al., 2019). However, correlating palynomorphs over such a large area introduces additional uncertainty due to the potential for floral provincialism and paleoecologic succession, which has the potential to introduce diachronous palynostratigraphic records (Barbolini et al., 2016). Further difficulties arise with the fact that these strata represent alluvial depositional systems affected by channelized erosional surfaces, so as to make uncertain the completeness of the sedimentary record.

In non-marine succession of Eastern Australia, the PTB was positioned at the top of the uppermost coal bed and at the base of coarse-grained sandstones (Foster et al., 1998; Michaelsen, 2002; Metcalfe et al., 2015). However, in the outcrops where the shale overlying the uppermost coal seam is preserved, geochemical evidence constrains the EPE ca. 1 m above the coal top (Williams et al., 2017). Fielding et al. (2019), based on U—Pb data, indicate an age of 252.31 ± 0.07 Ma for the EPE in the Sydney Basin, which is ~410,000 years older than the PTB of the GSSP. Fielding et al. (2019) and Mays et al. (2020) further indicate a terrestrial extinction preceding the marine EPE by ~370 ky (Burgess et al., 2014; Zhang et al., 2016; Xu et al., 2017; Shen et al., 2019). This data indicates that terrestrial successions containing a preserved record of the EPE and PTB would likely show paleoenvironmental disruption in between the last occurrence of Permian flora/fauna and the first occurrence of Triassic flora/fauna, where the EPE and PTB would bracket this stratigraphic interval of paleoenvironmental disturbance.

Within the Beacon Supergroup of SVL, the stratigraphic position of the PTB has been deeply discussed in literature, leading to alternative interpretations: i) the boundary is placed between the Feather Conglomerate and the Mt. Fleming Member (Barrett and Kohn, 1975; Ballance, 1977; Barrett, 1981; Collinson et al., 1983; Elliot and Grimes, 2011); ii) the PTB is not preserved in SVL as the boundary between the Weller Coal Measures and the Feather Conglomerate is represented as a regional disconformity, meaning a significant lacuna (Collinson et al., 1994; Isbell and Cúneo, 1996); iii) the PTB is preserved in SVL, and it has the same position of point ii), but without a significant time-gap (Tewari et al., 2015); iv) the PTB is located a few meters below the lithostratigraphic boundary between the two formations, in correspondence with the appearance of berthierine-bearing paleosols, marking a short lacuna, or absence of a lacuna (Retallack and Krull, 1999; Sheldon and Retallack, 2002; Retallack et al., 2005).

However, in the continental realm, the lithostratigraphic and biostratigraphic features usually considered marking the PTB (i.e., disappearance of glossopterid flora and termination of peat-forming conditions marked by the disappearance of coal beds) have been recently considered as indicative of the terrestrial EPE which would predate the PTB, as outlined in the Australian basins (Fielding et al., 2019; Gastaldo et al., 2020; Mays et al., 2020).

This study highlights the substantial conformable character of the boundary between the Weller Coal Measures and the Feather Conglomerate through a "transitional interval"; moreover, the palynostratigraphic data suggesting the possible presence of upper Permian strata (Awatar et al., 2014; Corti, 2021), strengthen the possibility that the PTB is recorded within the succession of Allan Hills, as well as of the SVL. To this respect, the lower to middle part of the subunit b of the "transitional interval" shows the occurrence of *Glossopteris* flora and it could still be assigned to the Permian, while subunits c and d lack macrofossil content (Fig. 7). Thus, subunit b is a critical component of the "transitional interval" as it may contain a record of the EPE and may preserve the PTB within the subunit or at the contact with subunit c (Fig. 8).

In the studied section from Log South, in the middle part of the subunit b, *Glossopteris* leaf impressions have been recognized and, above that, a very thin (ca. 20 cm thick) coal bed occurs. This most likely indicates that the EPE is placed at the boundary between this last coal-carbonaceous strata and the overlying siltstone (at ca. 83 m in the log South, in the upper part of the subunit b; Figs. 4, 7, 8). Moreover, the EPE does not correspond with major lithological change, in agreement

with the conformable character of the successions, as well as has been pointed out in the Sydney Basin (Fielding et al., 2019, 2021). The EPE does not mark neither any change in the mineralogical composition of sandstones, which present characteristics of the PF2 (Fig. 4). This interval shows strong similarities with that observed in the Australian basins where the EPE has been clearly fixed (Fielding et al., 2019, 2021; Mays et al., 2020, 2021a, 2021b; McLoughlin et al., 2020, 2021; Vajda et al., 2020). The occurrence of charcoal fragments also in the upper part of Unit A resembles a catastrophic scenario characterized by paleo-fires which predate the EPE, similarly to what is proposed in the North China Plate (Cai et al., 2021; Lu et al., 2022), and the spike in paleo-fires activity in time equivalent strata in eastern Australia (Mays and McLoughlin, 2022).

The first report of the EPE in the Allan Hills succession allows us to constrain the occurrence of the PTB in the "transitional interval" between the units A and B, and more precisely in the uppermost part of the subunit b (Fig. 8). The jarosite occurring within concretions in the uppermost part of subunit b (Figs. 7, 8) is likely derived from the oxidation of pyrite and/or marcasite. Pyrite and jarosite are recorded at the Permian-Triassic boundary in Australia, South Africa, and Antarctica (Retallack and Alonso-Zarza, 1998; Retallack et al., 2005). The formation of pyrite in the sediments is indicative of reducing conditions; in the Sydney Basin Vajda et al. (2020) attributed the presence of pyrite, later altered into jarosite, to bacterial activity in the "dead zone", a stratigraphic interval above the EPE where pollens are absent while only wood fragments, charcoal, algal thalli, and fungal spores occur. The stratigraphic position of the jarosite-bearing concretions in the Allan Hills section, ca. 1 m above the EPE, is comparable with those of the Sydney Basin, which supports the hypothesis of a "dead zone" following the EPE also in this sector of Gondwana.

This tentatively assigned position of the PTB substantially agrees with the supposed position by Retallack et al. (2005) based on paleosols change, analogous to the central TAM (Retallack et al., 2007). Following these points, the "transitional interval" records the EPE and the PTB (subunit b), assigning the earliest Triassic age to subunits c and d, which correspond to the uppermost part of the Weller Coal Measures by a lithostratigraphic point of view.

6. Conclusions

The Allan Hills nunatak in southern Victoria Land preserves one of the best exposed and most complete Permian-Triassic fluvial sequences of this sector of Gondwana. Even if the sequence was deeply studied, this study provides new field stratigraphic and petrographic data which allow a reappraisal of the lithostratigraphy of Permian to Upper Triassic succession and the relationships among units, that led to a strengthening of the knowledge across the Permian-Triassic boundary in Antarctica.

The identification of six depositional-stratigraphic units (A to F), based on facies association occurrence, vertical stacking pattern, sedimentary structures, sandstone composition, and macrofossil flora content, allowed to refine a detailed lithostratigraphic frame for the Permian-Triassic sequence of Allan Hills, important for the whole SVL. The changes in the facies association assemblage across the whole succession testify paleoenvironmental changes across the Late Permian and Triassic, mainly related to climate variations and tectonic activity. Sandstone mineralogical composition records provenance changes, with transition from basin fed by intrusive and metamorphic basement during the Late Permian-Early Triassic interval, to a volcanic arc-fed basin during Middle-Late Triassic.

The bounding surfaces which delimitate the lithostratigraphic units do not constitute important erosion surfaces, emphasizing the substantial conformable attitude of the units and a potentially continuous alluvial sedimentary sequence through Permian and Triassic. In this context, the "transitional interval" between Weller Coal Measures (Unit A) and Feather Conglomerate (Unit B) assumes a key role. The "transitional interval" incorporates peculiar features of both units, even if it shows more lithological affinity with the Unit A (Weller Coal Measures). The "transitional interval" reveals a gradual and conformable lithostratigraphic passage, even if marked by minor erosional features, inherent in an alluvial depositional system. Moreover, the lithological/sedimentological features allow to infer the presence and the position of the continental end-Permian Extinction (EPE) episode in the Antarctic sequence. This is located at the top of the uppermost coal-carbonaceous bed within the "transitional interval", sharing several features with the well constrained successions of the Sydney Basin (Eastern Australia). The EPE shortly predates the Permian-Triassic boundary, which is inferred to be in the middle of the "transitional interval" that, from a lithostratigraphic point of view corresponds with the uppermost part of the Weller Coal Measures. The lithological and petrological features, the macroflora and the organic matter recovered in this study make the Allan Hills record, and the entire southern Victoria Land one, comparable with other southern Gondwana basins.

Declaration of Competing Interest

The authors declare that they have no known competing financial interests or personal relationships that could have appeared to influence the work reported in this paper.

Data availability

Data will be made available on request.

Acknowledgments

This work was mainly supported by the Italian "Programma Nazionale di Ricerca in Antartide" [grant number PNRA AZ2.08/2013]. We thank the personnel of the ENEA and of the whole Mario Zucchelli Station for their great and efficient support for base and field activities, especially for the coordination and set up of the remote camps, with a particular praise to our mountain guide Loris Buzzi, who patiently assisted us in the camp activities. Thanks also to the pilots of the Helicopters New Zealand and to the crew of the Twin Otter of the Kenn Borek Air, for their professionality and availability. We also thank Riccardo Salvini for a preliminary setting of satellite images and the Museo Nazionale dell'Antartide – Siena section. We are also grateful to the Editor Shuzhong Shen, the reviewers Christopher Fielding and an anonymous one for their extremely precious comments and suggestions.

Finally, we dedicate this paper to the memory of our friend and colleague Franco M. Talarico, that in a forward-looking way led us on this path.

Appendix A. Supplementary data

Supplementary data to this article can be found online at https://doi.org/10.1016/j.palaeo.2023.111741.

References

Askin, R.A., 1997. Victoria, Permian palynomorphs from southern Land, Antarctica. Antarct. J. United States 30, 47–48.

Awatar, R., Tewari, R., Agnihotri, D., Chatterjee, S., Pillai, S.S.K., Meena, K.L., 2014. Late Permian and Triassic palynomorphs from the Allan Hills, central Transantarctic Mountains, South Victoria Land, Antarctica. Curr. Sci. 106, 988–995.

Ballance, P.F., 1977. The Beacon supergroup in the Allan Hills, central Victoria Land, Antarctica. New Zeal. J. Geol. Geophys. 20, 1003–1116. https://doi.org/10.1080/00288306.1977.10420693.

Ballance, P.F., Watters, W.A., 1971. In: The Mawson Diamictite and the Carapace Sandstone, formations of the Ferrar Group at Allan Hills and Carapace Nunatak, Victoria Land, Antarctica, 14, pp. 512–527. https://doi.org/10.1080/00288306.1971.10421945.

Barbolini, N., Bamford, M.K., Rubidge, B., 2016. Radiometric dating demonstrates that Permian spore-pollen zones of Australia and South Africa are diachronous. Gondwana Res. 37, 241–251. https://doi.org/10.1016/j.gr.2016.06.006.

Barrett, P.J., 1981. History of the Ross Sea region during the deposition of the Beacon Supergroup 400–180 million years ago. J. R. Soc. New Zeal. 11, 447–458. https://doi.org/10.1080/03036758.1981.10423334.
Barrett, P.J., 1991. The Devonian to Jurassic Beacon Supergroup of the Transantarctic Mountains and correlatives in other parts of Antarctica. In: Tingey, R.J. (Ed.), The Geology of Antarctica. Clarendon Press, Oxford, pp. 120–152.
Barrett, P.J., Fitzgerald, P.G., 1985. Deposition of the lower Feather Conglomerate, a Permian braided river deposit in Southern Victoria Land, Antarctica, with notes on the regional paleogeography. Sediment. Geol. 45, 189–208.
Barrett, P.J., Kohn, B.P., 1975. Changing sediment transport directions from Devonian to Triassic in the Beacon Supergroup of South Victoria Land, Antarctica. In: Campbell, K.S.W. (Ed.), Gondwana Geology. A.N.U. Press, Camberra, pp. 15–35.
Barrett, P.J., Kohn, B.P., Askin, R.A., McPherson, J.G., 1971. Preliminary report on Beacon Supergroup studies between the Hatherton and Mackay Glaciers, Antarctica. New Zeal. J. Geol. Geophys. 14, 605–614. https://doi.org/10.1080/00288306.1971.10421951.
Barrett, P.J., Webb, P.N., 1973. Stratigraphic sections of the Beacon Supergroup (Devonian and older (?) to Jurassic) in South Victoria Land. In: Publication of the Geology Department. Victoria University of Wellington, pp. 1–165.
Bomfleur, B., Krings, M., Kaštovský, J., Kerp, H., 2009. An enigmatic non-marine thalloid organism from the Triassic of East Antarctica. Rev. Palaeobot. Palynol. 157, 317–325. https://doi.org/10.1016/J.REVPALBO.2009.06.004.
Bomfleur, B., Mörs, T., Unverfärth, J., Liu, F., Läufer, A., Castillo, P., Oh, C., Park, T.-Y.S., Woo, J., Crispini, L., 2021. Uncharted Permian to Jurassic continental deposits in the far north of Victoria Land, East Antarctica. J. Geol. Soc. Lond. 178 https://doi.org/10.1144/jgs2020-062.
Borns, H.W., Hall, B.A., 1969. Mawson "Tillite" in Antarctica: preliminary Report of a Volcanic Deposit of Jurassic Age. Science 166, 870–872. https://doi.org/10.1126/SCIENCE.166.3907.870.
Brand, U., Posenato, R., Came, R., Affek, H., Angiolini, L., Azmy, K., Farabegoli, E., 2012. The end-Permian mass extinction: a rapid volcanic CO2 and CH4-climatic catastrophe. Chem. Geol. 322–323, 121–144. https://doi.org/10.1016/J.CHEMGEO.2012.06.015.
Burgess, S.D., Bowring, S., Shen, S.Z., 2014. High-precision timeline for Earth's most severe extinction. Proc. Natl. Acad. Sci. U. S. A. 111, 3316–3321. https://doi.org/10.1073/PNAS.1317692111/SUPPL_FILE/2015COZZ-CLASS-1.MP4.
Burgess, S.D., Muirhead, J.D., Bowring, S.A., 2017. Initial pulse of Siberian Traps sills as the trigger of the end-Permian mass extinction. Nat. Commun. 81 (8), 1–6. https://doi.org/10.1038/s41467-017-00083-9.
Burns, C.E., Mountney, N.P., Hodgson, D.M., Colombera, L., 2019. Stratigraphic architecture and hierarchy of fluvial overbank splay deposits. J. Geol. Soc. Lond. 176, 629–649. https://doi.org/10.1144/JGS2019-001/ASSET/0F2527D1-B0CA-45DD-8E67-41AF66C0C220/ASSETS/IMAGES/LARGE/JGS2019-001.13.JPG.
Cai, Y., Zhang, H., Cao, C., Zheng, Q., Jin, C., Shen, S., 2021. Wildfires and deforestation during the Permian-Triassic transition in the southern Junggar Basin, Northwest China. Earth-Sci. Rev. 218, 103670 https://doi.org/10.1016/J.EARSCIREV.2021.103670.
Collinson, J.W., Hammer, W.R., Askin, R.A., Elliot, D.H., 2006. Permian-Triassic boundary in the central Transantarctic Mountains, Antarctica. GSA Bull. 118, 747–763. https://doi.org/10.1130/B25739.1.
Collinson, J.W., Isbell, J.L., Elliot, D.H., Miller, M.F., Miller, J.M.G., Veevers, J.J., 1994. Permian-Triassic Transantarctic basin. In: Veevers, J.J., Powell, C.M.A. (Eds.), Permian-Triassic Pangean Basins and Foldbelt along the Panthalassan Marfin of Gondwanaland. Geological Society of America Memoir, Boulder, Colorado, pp. 173–222. https://doi.org/10.1130/MEM184-p173.
Collinson, J.W., Pennington, D.C., Kemp, N.R., 1983. Sedimentary petrology of Permian-Triassic fluvial rocks in Allan Hills, central Victoria Land. Antarct. J. United States 18, 20–22.
Cornamusini, G., Corti, V., Liberato, G.P., Perotti, M., Sandroni, S., Talarico, F.M., 2020. Foreste Fossili in Antartide. Geologicamente 1, 27–35. https://doi.org/10.3301/GM.2020.01.
Cornamusini, G., Talarico, F.M., Cirilli, S., Spina, A., Olivetti, V., Woo, J., 2017. Upper Paleozoic glacigenic deposits of Gondwana: Stratigraphy and paleoenvironmental significance of a tillite succession in Northern Victoria Land (Antarctica). Sediment. Geol. 358, 51–69. https://doi.org/10.1016/j.sedgeo.2017.07.002.
Corti, V., 2021. Palynology and Paleobotany of Permo-Triassic Beacon Supergroup at Allan Hills, South Victoria Land, Antarctica: stratigraphical and paleoenvironmental change implications (Ph.D. thesis). University of Siena, Siena, 198 pp.
Cox, S.C., Turnbull, I.M., Isaac, M.J., Townsend, D.B., Lyttle, B.S., 2012. Geology of southern Victoria Land, Antarctica, Institute of Geological & Nuclear Sciences 1:250 000 geological map 22. 1 sheet + 135 pp. GNS Science, Lower Hutt, New Zealand.
Cùneo, N.R., Isbell, J., Taylor, E.L., Taylor, T.N., 1993. The Glossopteris Flora in Antarctica: taphonomy and paleoecology. Compt. Rend. 2, 13–40.
Dal Corso, J., Mills, B.J.W., Chu, D., Newton, R.J., Mather, T.A., Shu, W., Wu, Y., Tong, J., Wignall, P.B., 2020. Permo–Triassic boundary carbon and mercury cycling linked to terrestrial ecosystem collapse. Nat. Commun. 111 (11), 1–9. https://doi.org/10.1038/s41467-020-16725-4.
Dalrymple, R.W., 1992. Tidal Depositional Systems. In: Walker, R.G., James, N.P. (Eds.), Facies Models: Response to Sea Level Change. Geological Association of Canada, Newfoundland, pp. 195–218.
Decombeix, A.L., Taylor, E.L., Taylor, T.N., 2012. Gymnosperm trees from the Permian of Antarctica: an anatomically preserved trunk of Kaokoxylon sp. Compt. Rend. Palevol. 11, 21–29. https://doi.org/10.1016/J.CRPV.2011.10.002.
Decombeix, A.L., Taylor, E.L., Taylor, T.N., 2009. In: Secondary Growth in Vertebraria Roots from the Late Permian of Antarctica: A Change in Developmental Timin, 170, pp. 644–656. https://doi.org/10.1086/597784.
Dickinson, W.R., 1985. Interpreting provenance relations from detrital modes of sandstones. In: Zuffa, G.G. (Ed.), Provenance of Arenites. NATO ASI, Dordrecht, pp. 333–361. https://doi.org/10.1007/978-94-017-2809-6_15/COVER.
Elliot, D.H., 2013. The geological and tectonic evolution of the Transantarctic Mountains: a review. Geol. Soc. London, Spec. Publ. 381, 7–35. https://doi.org/10.1144/SP381.14.
Elliot, D.H., Fortner, E.H., Grimes, C.B., 2006. Mawson Breccias Intrude Beacon Strata at Allan Hills, South Victoria Land: Regional Implications. In: Fütterer, D.K., Damaske, D., Kleinschmidt, G., Miller, H., Tessensohn, F. (Eds.), Antarctica: Contributions to Global Earth Sciences. Springer, Berlin, pp. 291–298. https://doi.org/10.1007/3-540-32934-X_36.
Elliot, D.H., Grimes, C.G., 2011. Triassic and Jurassic strata at Coombs Hills, South Victoria Land: stratigraphy, petrology and cross-cutting breccia pipes. Antarct. Sci. 23, 268–280. https://doi.org/10.1017/S0954102010000994.
Elliot, D.H., Larsen, D., Fanning, C.M., Fleming, T.H., Vervoort, J.D., 2017. The lower Jurassic Hanson Formation of the Transantarctic Mountains: implications for the Antarctic sector of the Gondwana plate margin. Geol. Mag. 154, 777–803. https://doi.org/10.1017/S0016756816000388.
Escapa, I.H., Taylor, E.L., Cúneo, R., Bomfleur, B., Bergene, B., Serbet, R., Taylor, T.N., 2011. Triassic floras of Antarctica: plant diversity and distribution in high paleolatitude communitieS. Palaios 26, 522–544. https://doi.org/10.2110/PALO.2010.P10-122R.
Eze, P.N., Udeigwe, T.K., Meadows, M.E., 2014. Plinthite and its Associated Evolutionary Forms in Soils and Landscapes: a Review. Pedosphere 24, 153–166. https://doi.org/10.1016/S1002-0160(14)60002-3.
Farabee, M.J., Taylor, E.L., Taylor, T.N., 1990. Correlation of permian and triassic palynomorph assemblages from the central Transantarctic Mountains, Antarctica. Rev. Palaeobot. Palynol. 65, 257–265. https://doi.org/10.1016/0034-6667(90)90075-T.
Fielding, C.R., Alexander, J., Allen, J.P., 2018. The role of discharge variability in the formation and preservation of alluvial sediment bodies. Sediment. Geol. 365, 1–20. https://doi.org/10.1016/J.SEDGEO.2017.12.022.
Fielding, C.R., Frank, T.D., McLoughlin, S., Vajda, V., Mays, C., Tevyaw, A.P., Winguth, A., Winguth, C., Nicoll, R.S., Bocking, M., Crowley, J.L., 2019. Age and pattern of the southern high-latitude continental end-Permian extinction constrained by multiproxy analysis. Nat. Commun. 10, 385. https://doi.org/10.1038/s41467-018-07934-z.
Fielding, C.R., Frank, T.D., Tevyaw, A.P., Savatic, K., Vajda, V., McLoughlin, S., Mays, C., Nicoll, R.S., Bocking, M., Crowley, J.L., 2021. Sedimentology of the continental end-Permian extinction event in the Sydney Basin, eastern Australia. Sedimentology 68, 30–62. https://doi.org/10.1111/sed.12782.
Fielding, C.R., Stephens, C.J., Holcombe, R.J., 1997. Permian stratigraphy and palaeogeography of the eastern Bowen Basin, Gogango Overfolded Zone and Strathmuir Synclinorium in the Rockhampton-Mackay region, central Queensland. In: Ashley, P.M., Flood, P.G. (Eds.), Tectonics and Metallogenesis o/the New England Orogen. Geological Society of Australia Special Publication, pp. 80–95.
Fitzgerald, P.G., Barrett, P.J., 1986. Skolithos in a Permian braided river deposit, southern Victoria Land, Antarctica. Palaeogeogr. Palaeoclimatol. Palaeoecol. 52, 237–247. https://doi.org/10.1016/0031-0182(86)90049-0.
Foster, C.B., Logan, G.A., Summons, R.E., 1998. The Permian-Triassic boundary in Australia: where is it and how is it expressed? Proc. R. Soc. Victoria 110, 247–266.
Gabites, H.I., 1985. Triassic Paleoecology of the Lashly Formation, Transantarctic Mts., Antarctica. Victoria University of Wellington.
Garzanti, E., 2019. Petrographic classification of sand and sandstone. Earth-Sci. Rev. 192, 545–563. https://doi.org/10.1016/J.EARSCIREV.2018.12.014.
Gastaldo, R.A., Kamo, S.L., Neveling, J., Geissman, J.W., Looy, C.V., Martini, A.M., 2020. The base of the Lystrosaurus Assemblage Zone, Karoo Basin, predates the end-Permian marine extinction. Nat. Commun. 11, 1428. https://doi.org/10.1038/s41467-020-15243-7.
Gazzi, P., 1966. Mineral. Petrogrographica Acta 12, 69–97.
Gibling, M.R., Bashforth, A.R., Falcon-Lang, H.J., Allen, J.P., Fielding, C.R., 2010. Log Jams and Flood Sediment Buildup Caused Channel Abandonment and Avulsion in the Pennsylvanian of Atlantic Canada. J. Sediment. Res. 80, 268–287. https://doi.org/10.2110/JSR.2010.024.
Goodge, J.W., 2020. Geological and tectonic evolution of the Transantarctic Mountains, from ancient craton to recent enigma. Gondwana Res. 80, 50–122. https://doi.org/10.1016/j.gr.2019.11.001.
Gugliotta, M., Flint, S.S., Hodgson, D.M., Veiga, G.D., 2016. Recognition criteria, characteristics and implications of the fluvial to marine transition zone in ancient deltaic deposits (Lajas Formation, Argentina). Sedimentology 63, 1971–2001. https://doi.org/10.1111/SED.12291.
Gulbranson, E.L., Cornamusini, G., Ryberg, P.E., Corti, V., 2020. When does large woody debris influence ancient rivers? Dendrochronology applications in the Permian and Triassic, Antarctica. Palaeogeogr. Palaeoclimatol. Palaeoecol. 541, 109544 https://doi.org/10.1016/j.palaeo.2019.109544.
Gulbranson, E.L., Isbell, J.L., Taylor, E.L., Ryberg, P.E., Taylor, T.N., Flaig, P.P., 2012. Permian polar forests: deciduousness and environmental variation. Geobiology 10, 479–495. https://doi.org/10.1111/J.1472-4669.2012.00338.X.
Gulbranson, E.L., Mellum, M.M., Corti, V., Dahlseid, A., Atkinson, B.A., Ryberg, P.E., Cornamusini, G., 2022a. Paleoclimate-induced stress on polar forested ecosystems prior to the Permian-Triassic mass extinction. Sci. Rep. 12, 1–13. https://doi.org/10.1038/s41598-022-12842-w.
Gulbranson, E.L., Ryberg, P.E., Decombeix, A.L., Taylor, E.L., Taylor, T.N., Isbell, J.L., 2014. Leaf habit of Late Permian Glossopteris trees from high-palaeolatitude forests. J. Geol. Soc. London. 171, 493–507. https://doi.org/10.1144/JGS2013-127.

Gulbranson, E.L., Sheldon, N.D., Montañez, I.P., Tabor, N.J., McIntosh, J.A., 2022b. Late Permian soil-forming paleoenvironments on Gondwana: a review. Palaeogeogr. Palaeoclimatol. Palaeoecol. 586, 110762 https://doi.org/10.1016/J.PALAEO.2021.110762.

Gunn, B.M., Warren, G., 1962. Geology of Victoria Land between the Mawson and Mulock Glaciers, Antarctica. New Zeal. Geol. Surv. Bull. 71, 1–157.

Harrington, H.J., 1965. Geology and morphology of Antarctica. In: Van Oye, P., Van Mieghen, J. (Eds.), Biogeography and Ecology in Antarctica, pp. 1–71.

Ingersoll, R.V., Bullard, T.F., Ford, R.L., Grimm, J.P., Pickle, J.D., Sares, S.W., 1984. The effect of grain size on detrital modes: a test of the Gazzi-Dickinson point-counting method. J. Sediment. Res. 54, 103–116. https://doi.org/10.1306/212F83B9-2B24-11D7-8648000102C1865D.

Isbell, J.L., Cúneo, N.R., 1996. Depositional framework of Permian coal-bearing strata, southern Victoria Land, Antarctica. Palaeogeogr. Palaeoclimatol. Palaeoecol. 125, 217–238. https://doi.org/10.1016/S0031-0182(96)00032-6.

Ives, L.R.W., Isbell, J.L., 2021. A lithofacies analysis of a South Polar glaciation in the Early Permian: Pagoda Formation, Shackleton Glacier region, Antarctica. J. Sediment. Res. 91, 611–635. https://doi.org/10.2110/jsr.2021.004.

Kaczorek, D., Sommer, M., 2003. Micromorphology, chemistry, and mineralogy of bog iron ores from Poland. Catena 54, 393–402. https://doi.org/10.1016/S0341-8162(03)00133-4.

Kaczorek, D., Sommer, M., Andruschkewitsch, I., Oktaba, L., Czerwinski, Z., Stahr, K., 2004. A comparative micromorphological and chemical study of "Raseneisenstein" (bog iron ore) and "Ortstein". Geoderma 121, 83–94. https://doi.org/10.1016/J.GEODERMA.2003.10.005.

Kyle, R.A., 1977. Palynostratigraphy of the Victoria Group of South Victoria Land, Antarctica. New Zeal. J. Geol. Geophys. 20, 1081–1102. https://doi.org/10.1080/00288306.1977.10420697.

Kyle, R.A., Schopf, J.M., 1982. Permian and Triassic palynostratigraphy of the Victoria Group, Transantarctic Mountains. In: Craddock, C. (Ed.), Antarctic Geoscience. University of Wisconsin Press, Madison, pp. 649–659.

Liberato, G.P., Cornamusini, G., Perotti, M., Sandroni, S., Talarico, F.M., 2017. Stratigraphy of a Permian-Triassic fluvial-dominated succession in Southern Victoria Land (Antarctica): preliminary data. J. Mediterr. Earth Sci. 9, 167–171.

Lu, J., Wang, Y., Yang, M., Zhang, P., Bond, D.P.G., Shao, L., Hilton, J., 2022. Diachronous end-Permian terrestrial ecosystem collapse with its origin in wildfires. Palaeogeogr. Palaeoclimatol. Palaeoecol. 594, 110960 https://doi.org/10.1016/j.palaeo.2022.110960.

Mays, C., McLoughlin, S., 2022. End-Permian burnout: the role of Permian-Triassic wildsfires in extinction, carbon cycling, and environmental change in eastern Gondwana. Palaios 37, 292–317. https://doi.org/10.2110/PALO.2021.051.

Mays, C., McLoughlin, S., Frank, T.D., Fielding, C.R., Slater, S.M., Vajda, V., 2021a. Lethal microbial blooms delayed freshwater ecosystem recovery following the end-Permian extinction. Nat. Commun. 12, 5511. https://doi.org/10.1038/s41467-021-25711-3.

Mays, C., Vajda, V., Frank, T.D., Fielding, C.R., Nicoll, R.S., Tevyaw, A.P., McLoughlin, S., 2020. Refined Permian-Triassic floristic timeline reveals early collapse and delayed recovery of south polar terrestrial ecosystems. Bull. Geol. Soc. Am. 132, 1489–1513. https://doi.org/10.1130/B35355.1.

Mays, C., Vajda, V., McLoughlin, S., 2021b. Permian-Triassic non-marine algae of Gondwana—Distributions, natural affinities and ecological implications. Earth-Sci. Rev. 212, 103382 https://doi.org/10.1016/j.earscirev.2020.103382.

McBride, E.F., 1963. A classification of common sandstones. J. Sediment. Res. 33, 664–669. https://doi.org/10.1306/74D70EE8-2B21-11D7-8648000102C1865D.

McElroy, C.T., 1969. Comparative lithostratigraphy of Gondwana sequences, eastern Australia and Antarctica. In: Amos, A.J. (Ed.), Gondwana Stratigraphy, pp. 441–466. Paris.

McLoughlin, S., Mays, C., Vajda, V., Bocking, M., Frank, T.D., Fielding, C.R., 2020. Dwelling in the dead zone-vertebrate burrows immediately succeeding the end-permian extinction event in Australia. Palaios 35, 342–357. https://doi.org/10.2110/PALO.2020.007.

McLoughlin, S., Nicoll, R.S., Crowley, J.L., Vajda, V., Mays, C., Fielding, C.R., Frank, T.D., Wheeler, A., Bocking, M., 2021. Age and Paleoenvironmental Significance of the Frazer Beach Member—A New Lithostratigraphic Unit Overlying the End-Permian Extinction Horizon in the Sydney Basin, Australia. Front. Earth Sci. 8, 600976 https://doi.org/10.3389/feart.2020.600976.

Metcalfe, I., Crowley, J.L., Nicoll, R.S., Schmitz, M., 2015. High-precision U-Pb CA-TIMS calibration of Middle Permian to lower Triassic sequences, mass extinction and extreme climate-change in eastern Australian Gondwana. Gondwana Res. 28, 61–81. https://doi.org/10.1016/J.GR.2014.09.002.

Miall, A.D., 2006. The Geology of Fluvial Deposits, The Geology of Fluvial Deposits. Springer, Berlin. https://doi.org/10.1007/978-3-662-03237-4.

Miall, A.D., 1996. The geology of fluvial deposits : sedimentary facies, basin analysis, and petroleum geology, 582.

Miall, A.D., 1985. Architectural-element analysis: a new method of facies analysis applied to fluvial deposits. Earth-Sci. Rev. 22, 261–308. https://doi.org/10.1016/0012-8252(85)90001-7.

Miall, A.D., 1978. Fluvial Sedimentology, Geological Magazine. Canadian Society of Petroleum Geologists, Calgary. https://doi.org/10.1017/S0016756800044101.

Michaelsen, P., 2002. Mass extinction of peat-forming plants and the effect on fluvial styles across the Permian-Triassic boundary, northern Bowen Basin, Australia. Palaeogeogr. Palaeoclimatol. Palaeoecol. 179, 173–188. https://doi.org/10.1016/S0031-0182(01)00413-8.

Montañez, I.P., 2022. Current synthesis of the penultimate icehouse and its imprint on the Upper Devonian through Permian stratigraphic record. Geol. Soc. London, Spec. Publ. 512, 213–245. https://doi.org/10.1144/SP512-2021-124.

Payne, J.L., Clapham, M.E., 2012. End-Permian Mass Extinction in the Oceans: an Ancient Analog for the Twenty-first Century? Annu. Rev. Earth Planet. Sci. 40, 89–111. https://doi.org/10.1146/ANNUREV-EARTH-042711-105329.

Plink-Björklund, P., 2005. Stacked fluvial and tide-dominated estuarine deposits in high-frequency (fourth-order) sequences of the Eocene Central Basin, Spitsbergen. Sedimentology 52, 391–428. https://doi.org/10.1111/J.1365-3091.2005.00703.X.

Retallack, G.J., Alonso-Zarza, A.M., 1998. Middle Triassic Paleosols and paleoclimate of Antarctica. J. Sediment. Res. 68, 169–184. https://doi.org/10.2110/JSR.68.169.

Retallack, G.J., Greaver, T., Jahren, A.H., 2007. Return to Coalsack Bluff and the Permian-Triassic boundary in Antarctica. Glob. Planet. Change 55, 90–108. https://doi.org/10.1016/j.gloplacha.2006.06.017.

Retallack, G.J., Jahren, A.H., Sheldon, N.D., Chakrabarti, R., Metzger, C.A., Smith, R.M.H., 2005. The Permian-Triassic boundary in Antarctica. Antarct. Sci. 17, 241–258. https://doi.org/10.1017/S0954102005002658.

Retallack, G.J., Krull, E.S., 1999. Landscape ecological shift at the Permian-Triassic boundary in Antarctica. Aust. J. Earth Sci. 46, 785–812. https://doi.org/10.1046/j.1440-0952.1999.00745.x.

Sheldon, N.D., Retallack, G.J., 2002. Low oxygen levels in earliest Triassic soils: comment. Geology 30, 919–922. https://doi.org/10.1130/0091-7613(2002)030<0919:LOLIET>2.0.CO;2.

Shen, S.Z., Ramezani, J., Chen, J., Cao, C.Q., Erwin, D.H., Zhang, H., Xiang, L., Schoepfer, S.D., Henderson, C.M., Zheng, Q.F., Bowring, S.A., Wang, Y., Li, X.H., Wang, X.D., Yuan, D.X., Zhang, Y.C., Mu, L., Wang, J., Wu, Y.S., 2019. A sudden end-Permian mass extinction in South China. GSA Bull. 131, 205–223. https://doi.org/10.1130/B31909.1.

Smith, N.D., Barrett, P.J., Woolfe, K.J., 1998. Glacier-fed(?) sandstone sheets in the Weller Coal Measures (Permian), Allan Hills, Antarctica. Palaeogeogr. Palaeoclimatol. Palaeoecol. 141, 35–51. https://doi.org/10.1016/S0031-0182(98)00006-6.

Song, Haijun, Wignall, P.B., Chu, D., Tong, J., Sun, Y., Song, Huyue, He, W., Tian, L., 2014. Anoxia/high temperature double whammy during the Permian-Triassic marine crisis and its aftermath. Sci. Reports 41 (4), 1–7. https://doi.org/10.1038/srep04132.

Stump, E., 1995. In: The Ross Orogen of the Transantarctic Mountains. Cambridge University Press, Cambridge, p. 284.

Tewari, R., Chatterjee, S., Agnihotri, D., Pandita, S.K., 2015. Glossopteris flora in the Permian Weller Formation of Allan Hills, South Victoria Land, Antarctica: Implications for paleogeography, paleoclimatology, and biostratigraphic correlation. Gondwana Res. 28, 905–932. https://doi.org/10.1016/J.GR.2015.02.003.

Townrow, J.A., 1967. Fossil plants from Allan and Carapace Nunataks, and from the upper Mill and Shackleton Glaciers, Antarctica. New Zeal. Hournal Geol. Geophys. 10, 456–473. https://doi.org/10.1080/00288306.1967.10426750.

Vajda, V., McLoughlin, S., Mays, C., Frank, T.D., Fielding, C.R., Tevyaw, A., Lehsten, V., Bocking, M., Nicoll, R.S., 2020. End-Permian (252 Mya) deforestation, wildfires and flooding—An ancient biotic crisis with lessons for the present. Earth Planet. Sci. Lett. 529, 115875 https://doi.org/10.1016/j.epsl.2019.115875.

Webb, P.N., 1963. Geological investigations in southern Victoria land, Antarctica. New Zeal. J. Geol. Geophys. 6, 361–387. https://doi.org/10.1080/00288306.1963.10422069.

Williams, M.L., Jones, B.G., Carr, P.F., 2017. The interplay between massive volcanism and the local environment: Geochemistry of the Late Permian mass extinction across the Sydney Basin, Australia. Gondwana Res. 51, 149–169. https://doi.org/10.1016/J.GR.2017.07.015.

Wu, Y., Chu, D., Tong, J., Song, Haijun, Dal Corso, J., Wignall, P.B., Song, Huyue, Du, Y., Cui, Y., 2021. Six-fold increase of atmospheric pCO2 during the Permian–Triassic mass extinction. Nat. Commun. 121 (12), 1–8. https://doi.org/10.1038/s41467-021-22298-7.

Xu, G., Feng, Q., Deconinck, J.F., Shen, J., Zhao, T., Young, A.L., 2017. High-resolution clay mineral and major elemental characterization of a Permian-Triassic terrestrial succession in southwestern China: Diagenetic and paleoclimatic/paleoenvironmental significance. Palaeogeogr. Palaeoclimatol. Palaeoecol. 481, 77–93. https://doi.org/10.1016/J.PALAEO.2017.05.027.

Zhang, H., Cao, C.Q., Liu, X.L., Mu, L., Zheng, Q.F., Liu, F., Xiang, L., Liu, L.J., Shen, S.Z., 2016. The terrestrial end-Permian mass extinction in South China. Palaeogeogr. Palaeoclimatol. Palaeoecol. 448, 108–124. https://doi.org/10.1016/J.PALAEO.2015.07.002.

Zurli, L., Cornamusini, G., Woo, J., Liberato, G.P., Han, S., Kim, Y., Talarico, F.M., 2022. Detrital zircons from late Paleozoic Ice Age sequences in Victoria Land (Antarctica): New constraints on the glaciation of southern Gondwana. GSA Bull. 134, 160–178. https://doi.org/10.1130/B35905.1.